

# Analytic integration of singular kernels for boundary element analysis of plane orthotropic media

E. J. Barbero

West Virginia University, Morgantown USA

and

F. Vetere, A. Madeo <sup>1</sup>, and R. Zinno

University of Calabria, Arcavacata di Rende, CS, Italy

## Abstract

Both composite materials and stress concentration are common issues in modern structural engineering. In this paper, analytical integration of the singular kernels is performed for boundary element analysis (BEM) of elastic, plane orthotropic media with stress concentrations. Analytical integration leads to accuracy and efficiency improvements over FEM. Furthermore, high continuity (HC), quadratic spline interpolation on the boundary is used to further improve accuracy at low computational cost when compared to FEM. The advantages of BEM for calculation of displacements and stresses near stress raisers in orthotropic plates are shown. Particular attention is paid to efficient interpolation for approximating boundary quantities and to precision of computation for evaluating boundary integrals. Such improvements lead to accurate computation of both displacements and stresses in both the boundary and the domain. Thus, the advantages of the proposed method are accuracy and low computational cost.

## Keywords

Boundary Element Method (BEM), B. Elasticity, B. Stress concentrations, C. Computational modeling.

## 1 Introduction

Orthotropic materials, including laminated composite materials, are extensively used in modern industry. The theory of elasticity for orthotropic bodies is well established and solutions have been obtained for simple problems [1,2]. The presence of cracks increases the complexity of the analysis [3–7]. Therefore, complex problems of orthotropic, elastic bodies are analyzed with numerical methods, such as the Finite Element Method (FEM) [8–13] and the Boundary Element Method (BEM) [14–27]. Application examples of the BEM can be found, for example in [28–33]. Specific

---

<sup>1</sup>Corresponding author. The final publication is available at <http://dx.doi.org/10.1016/j.compositesb.2016.10.021>

application of BEM to plasticity and fracture can be found, for example in [34–37]. BEM analysis of interphase cracks and transverse isotropy in bimetals is presented in [38,39].

The boundary element approach can be used to construct efficient algorithms for numerical analysis of engineering problems. Some characteristics of this method are very attractive, namely the reduction of the dimension (e.g., from 2D to 1D) of the discrete model in comparison with domain methods (e.g., FEM), and the mixed nature (traction–displacement) of the method, which yields comparable accuracy in both displacements and tractions.

Green [40] first introduced the fundamental solutions for 2-D orthotropic bodies under a concentrated force. Rizzo and Shippy (1970) [41] introduced the fundamental solutions into the boundary integral equations for numerical elastic analysis of stress concentration. Recently, the fundamental solutions for orthotropic plane problems were improved [42–47], but numerical integration was used to compute the boundary coefficients.

Analytical evaluation of the boundary coefficients has been used for 2-D *isotropic*, plane and bending elastic problems [48–50] and in BEM for orthotropic, plane, potential problems [51,52]. In this paper, analytical integration is developed for the 2D *orthotropic* problem.

In the context of the boundary element method for plane orthotropic media, the aim of this work is to provide an accurate evaluation of the stress field with low computational cost. Accuracy and efficiency are achieved by refining both the boundary interpolation and the integration process. In summary, the boundary is discretized into macro-elements using a quadratic high continuity (HC) spline approximation to ensure  $C^1$  continuity using few control points. Then, analytical integration of coefficients is carried out on linear piecewise boundaries. The exact evaluation of integrals is decisive for an accurate, yet inexpensive computation of the domain stress field from the boundary solution. Finally, an assessment of the performance of the proposed methodology is presented.

## 2 Orthotropic plane problem

Consider a 2D orthotropic elastic body described in a rectangular Cartesian system  $x_1, x_2$ . The behavior of the body is described by two-dimensional fields of displacement, stress, and strain. The problem is governed by the customary equations, namely kinematic, constitutive, and equilibrium equations (e.g., [8, Chapter 2]).

### 2.1 Fundamental Solution

Consider an elastic orthotropic problem on a 2D infinite domain subjected to a concentrated force  $\mathbf{f}^*$  applied at the source point  $\xi$ . The fundamental solution for this problem is obtained by first rewriting the equilibrium equations, taking into account of the Hooke's law, into form

$$\mathbf{L}\mathbf{u} + \mathbf{b} = \mathbf{0} \quad (1)$$

where  $\mathbf{L}$  is the differential operator

$$[\mathbf{L}] = \begin{bmatrix} C_{11}\partial_1^2 + C_{66}\partial_2^2 & (C_{11} + C_{66})\partial_1\partial_2 \\ (C_{11} + C_{66})\partial_1\partial_2 & C_{22}\partial_2^2 + C_{66}\partial_1^2 \end{bmatrix} \quad (2)$$

and  $\mathbf{u}$  is the displacement field,  $\mathbf{b}$  are the body forces,  $\partial_i = \partial/\partial x_i$ , and  $C_{ij}$  are the coefficients of the stiffness tensor in Voigt contracted notation. Solving the system (2), the following fundamental solution was obtained by Huang [42], for displacements

$$\begin{aligned}
u_{11}^*(\xi, x) &= D [\sqrt{\lambda_1} A_2^2 \ln z_1 - \sqrt{\lambda_2} A_1^2 \ln z_2] \\
u_{12}^*(\xi, x) &= DA_1 A_2 \left[ \arctan \left( \frac{r_2}{\sqrt{\lambda_2} r_1} \right) - \arctan \left( \frac{r_2}{\sqrt{\lambda_1} r_1} \right) \right] \\
u_{21}^*(\xi, x) &= u_{12}(\xi, x) \\
u_{22}^*(\xi, x) &= -D \left[ \frac{A_1^2}{\sqrt{\lambda_1}} \ln z_1 - \frac{A_2^2}{\sqrt{\lambda_2}} \ln z_2 \right]
\end{aligned} \tag{3}$$

where the generic term  $u_{\alpha i}^*(\xi, x)$  of the fundamental solution represents the component of the displacement at the field point  $x$  in  $x_i$  direction due to the application at the source point  $\xi$  of a unit force directed along  $x_\alpha$ .

The fundamental solution for the tractions is

$$\begin{aligned}
t_{11}^*(\xi, x) &= D \left[ \frac{\sqrt{\lambda_2} A_1}{z_2^2} - \frac{\sqrt{\lambda_1} A_2}{z_1^2} \right] (r_1 n_1 + r_2 n_2) \\
t_{12}^*(\xi, x) &= D \left\{ \left( \frac{\sqrt{\lambda_1} A_1}{z_1^2} - \frac{\sqrt{\lambda_2} A_2}{z_2^2} \right) r_1 n_2 - \left( \frac{\sqrt{\lambda_1} A_1}{\lambda_1 z_1^2} - \frac{\sqrt{\lambda_2} A_2}{\lambda_2 z_2^2} \right) r_2 n_1 \right\} \\
t_{21}^*(\xi, x) &= D \left\{ \left( \frac{\lambda_1 \sqrt{\lambda_1} A_2}{z_1^2} - \frac{\lambda_2 \sqrt{\lambda_2} A_1}{z_2^2} \right) r_1 n_2 - \left( \frac{\sqrt{\lambda_1} A_2}{z_1^2} - \frac{\sqrt{\lambda_2} A_1}{z_2^2} \right) r_2 n_1 \right\} \\
t_{22}^*(\xi, x) &= D \left[ \frac{\sqrt{\lambda_1} A_1}{z_1^2} - \frac{\sqrt{\lambda_2} A_2}{z_2^2} \right] (r_1 n_1 + r_2 n_2)
\end{aligned} \tag{4}$$

where  $n_k$  represent the components of the unit normal at the field point  $x$ , and the generic term  $t_{\alpha i}^*(\xi, x)$  of the fundamental solution represents the component of the traction at the field point  $x$  in  $x_i$  direction due to the application at the source point  $\xi$  of a unit force directed along  $x_\alpha$ .

The distance between the source  $\xi$  and the field point  $x$  is

$$r_k(\xi, x) = x_k - \xi_k \tag{5}$$

where

$$\lambda_1 + \lambda_2 = \frac{2S_{12} + S_{66}}{S_{22}} \tag{6}$$

$$\lambda_1 \lambda_2 = \frac{S_{11}}{S_{22}} \tag{7}$$

$$A_k = S_{11} - \lambda_k S_{22} \tag{8}$$

$$z_k^2 = \lambda_k r_1^2 + r_2^2 \tag{9}$$

$$D = \frac{1}{2\pi(\lambda_1 - \lambda_2) S_{22}} \tag{10}$$

Equations (6) and (7) imply that

$$\lambda_{1,2} = \frac{2S_{21} + S_{66}}{2S_{22}} \pm \sqrt{\left(\frac{2S_{21} + S_{66}}{2S_{22}}\right)^2 - \left(\frac{S_{11}}{S_{22}}\right)} \quad (11)$$

where  $S_{ij}$  are the components of the compliance tensor in Voigt contracted notation.

## 2.2 Integral equation on the boundary

The integral equations on the boundary can be derived using Betti's reciprocal work theorem, or the weighted residuals method, resulting in Somigliana's equation [53]

$$\mathbf{u}(\xi) = \int_{\Gamma} \mathbf{u}^{*T}(\xi, x) \mathbf{t}(x) d\Gamma - \int_{\Gamma} \mathbf{t}^{*T}(\xi, x) \mathbf{u}(x) d\Gamma + \int_{\Omega} \mathbf{u}^{*T}(\xi, x) \mathbf{b}(x) d\Omega \quad (\xi \in \Gamma) \quad (12)$$

When evaluating (12) on the boundary, singularities of order  $O(1/r^2)$  require evaluation the integral as Cauchy Principal Values [54]

$$\mathbf{u}(\xi) = \int_{\Gamma} \mathbf{u}^{*T}(\xi, x) \mathbf{t}(x) d\Gamma - \left( \mathbf{M}_c^T \mathbf{u}(\xi) + \int_{\Gamma} \mathbf{t}^{*T}(\xi, x) \mathbf{u}(x) d\Gamma \right) + \int_{\Omega} \mathbf{u}^{*T}(\xi, x) \mathbf{b}(x) d\Omega \quad (\xi \in \Gamma) \quad (13)$$

which can be written as

$$\mathbf{c}^T \mathbf{u}(\xi) = \int_{\Gamma} \mathbf{u}^{*T}(\xi, x) \mathbf{t}(x) d\Gamma - \int_{\Gamma} \mathbf{t}^{*T}(\xi, x) \mathbf{u}(x) d\Gamma + \int_{\Omega} \mathbf{u}^{*T}(\xi, x) \mathbf{b}(x) d\Omega \quad (\xi \in \Gamma) \quad (14)$$

where  $\mathbf{b}$  are the body forces,  $\mathbf{u}^*$  and  $\mathbf{t}^*$  are the fundamental solutions (3) and (4),  $\Omega$  is the 2D domain,  $\Gamma$  is the boundary of the domain, and  $\mathbf{c}$  is  $2 \times 2$  coefficient matrix which depends on the surface geometry and it is defined as following

$$\mathbf{c} = \mathbf{I} + \mathbf{M}_c^T = \begin{bmatrix} 1 & 0 \\ 0 & 1 \end{bmatrix} + \begin{bmatrix} c_{11} & 0 \\ 0 & c_{22} \end{bmatrix} \quad (15)$$

where  $c_{11}$  and  $c_{22}$  are evaluated in the Appendix (4).

## 2.3 Discrete model

The approximate solution requires discretization of both the *geometry* of the contour and the *mechanical variables*, i.e., displacement and traction. The geometry of the contour can be represented through a system of curvilinear coordinates or through piecewise linearization. The curvilinear representation is the most general, but requires that the boundary integrals be evaluated numerically. Numerical integration requires us to pay particular attention to the calculation of singular and nearly singular integrals. On the other hand, a piecewise linear representation of the contour allows us to use analytical integration for both, the solution on the boundary  $\Gamma$  and the solution inside the domain  $\Omega$ .

For polygonal domains, the discretization into boundary elements proceeds as follows. The discontinuities of the boundary (e.g., corners) and the boundary conditions (e.g., attachment points) are used to subdivide the boundary into *macro-elements*. Macro-elements (denoted by  $M_i$  in Figure 1) are used to discretize the boundary; not the domain. In this way, the integral equations are

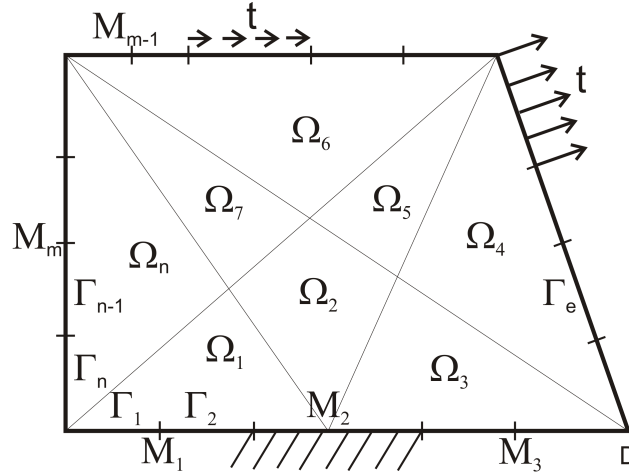


Figure 1: Discretization with macro-elements  $M_i$ , subdivided into elements  $\Gamma_e$ . Note that each change from a displacement boundary condition to a traction one, or viceversa, requires a new macro-element.

represented through summations extended over the number of macro-elements. Furthermore, the discretization of the mechanical variables on the boundary requires that each macro-element be subdivided into a finite number of evenly spaced elements (denoted by  $\Gamma_e$  in Figure 1).

The boundary variables are approximated by shape functions  $\phi_e(\zeta)$  (Figure 2) as follows

$$\begin{aligned}
 u(\zeta) &= \sum_{e=1}^{n_e} u_e(\zeta) = \sum_{e=1}^{n_e} \phi_{ue} u_e; & \phi_{ue} &= \left\{ \phi^{(j)}(\zeta), \phi^{(j+1)}(\zeta), \phi^{(j+2)}(\zeta) \right\} \\
 t(\zeta) &= \sum_{e=1}^{n_e} t_e(\zeta) = \sum_{e=1}^{n_e} \phi_{te} u_e; & \phi_{te} &= \left\{ \phi^{(j)}(\zeta), \phi^{(j+1)}(\zeta), \phi^{(j+2)}(\zeta) \right\}
 \end{aligned} \tag{16}$$

### 2.3.1 High Continuity (HC) Interpolation

The quality of the numerical solution depends on the quality of the representation of the variables on the boundary. An interpolation that has been shown to provide high quality interpolation is the *High Continuity (HC)* interpolation that was proposed by Aristodemo [55] and used for BEM in [48, 49].

In HC interpolation, the boundary variables are represented by a quadratic B-spline approximation which guarantees  $C^1$  continuity. In each element, the shape function is constructed using three control points (see Fig. 3(a)), associated with one node placed at the midpoint of the element itself, and one node on each of the two adjacent elements.

Each macro-element is divided into  $n$  elements. For  $n$  elements, while a piecewise constant interpolation uses  $n$  parameters, the HC interpolation HC uses  $n + 2$ . To enforce  $C^1$  continuity, while Hermite interpolation uses  $2n$  parameters, HC uses only  $n + 2$ , achieving the same continuity.

For  $n + 2$  parameters, HC interpolation requires  $n + 2$  sources located on the macro-element. The sources are located at the midpoint of the internal elements, plus one additional source for each of the end elements. The sources in the end elements are located as shown in Fig. (4), where  $\alpha = 0.6a$  and  $\beta = 1.4a$ , where  $a$  is the element half-length. The values of  $\alpha, \beta$ , are chosen by numerical optimization [49].

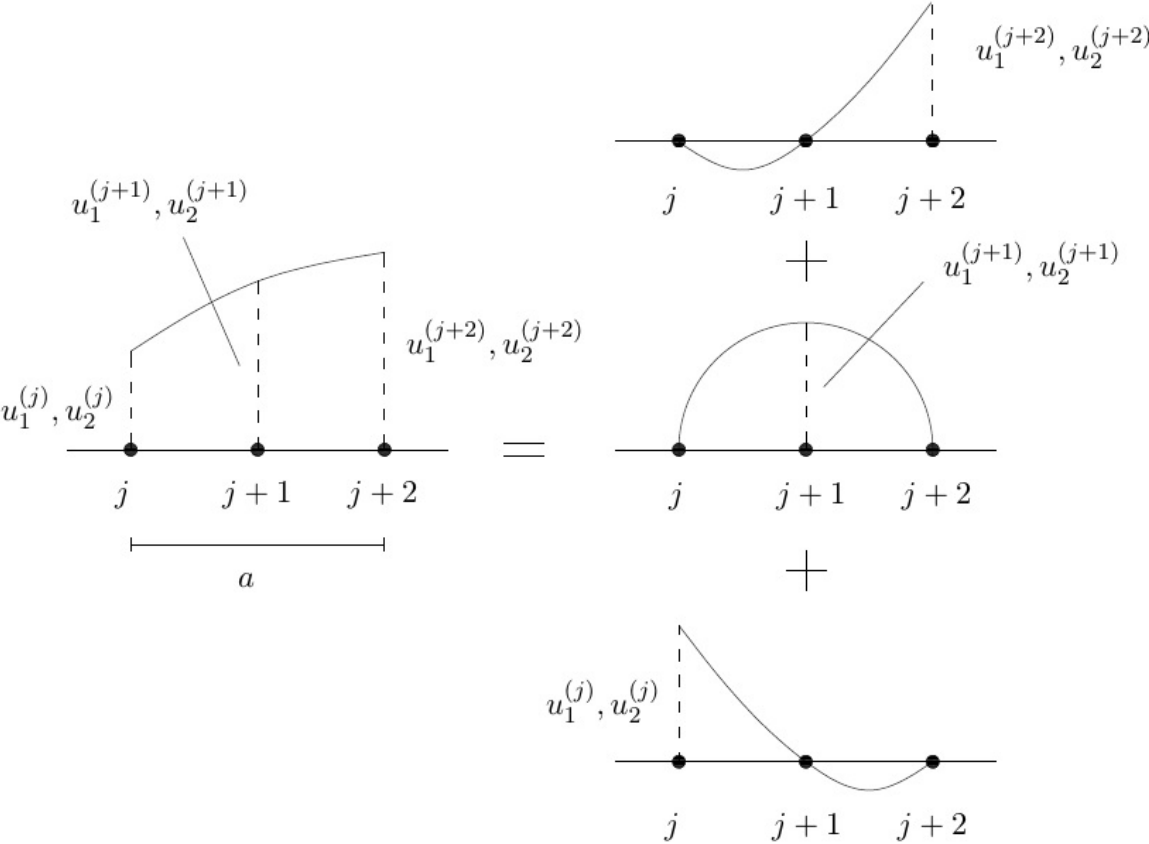


Figure 2: Quadratic interpolation of displacements.

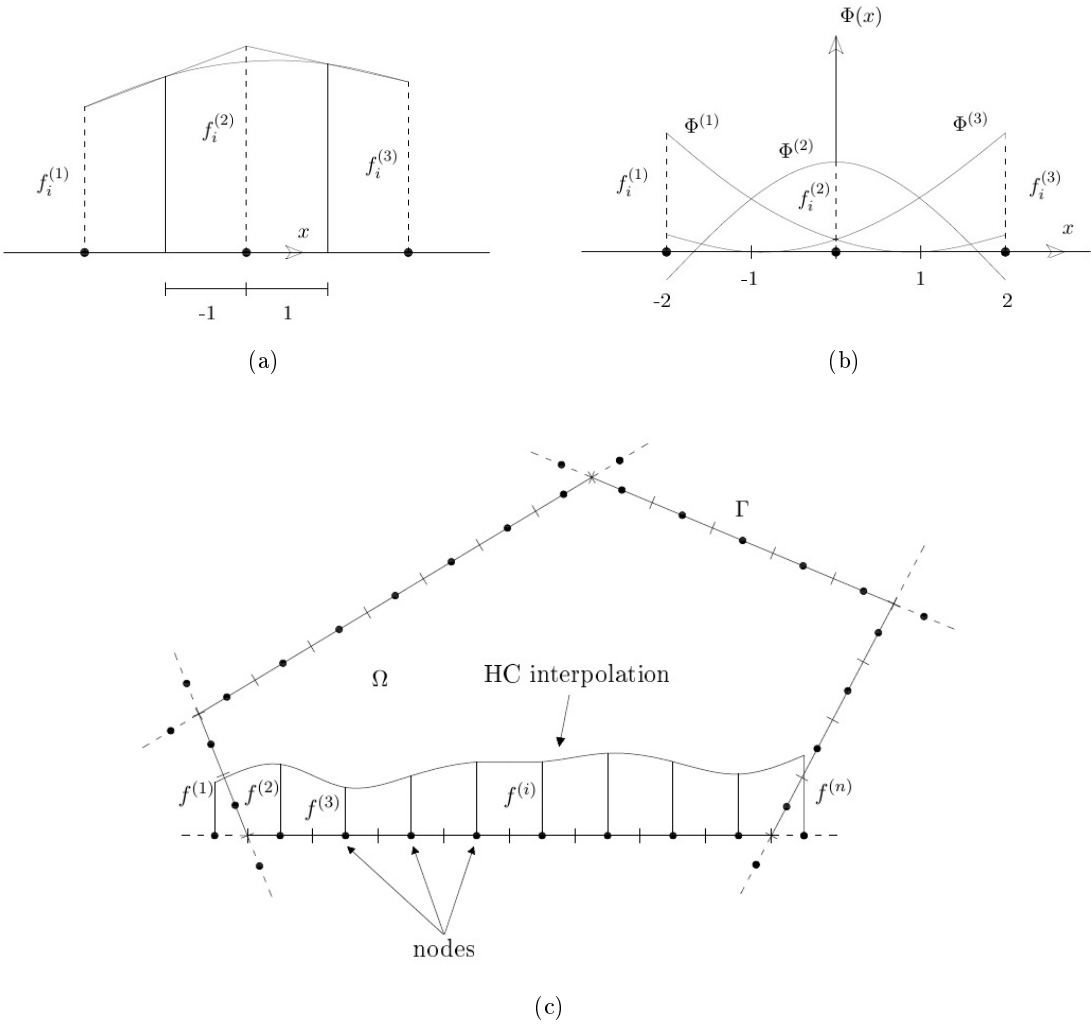


Figure 3: Shape functions and arrangement of the interpolation parameters.

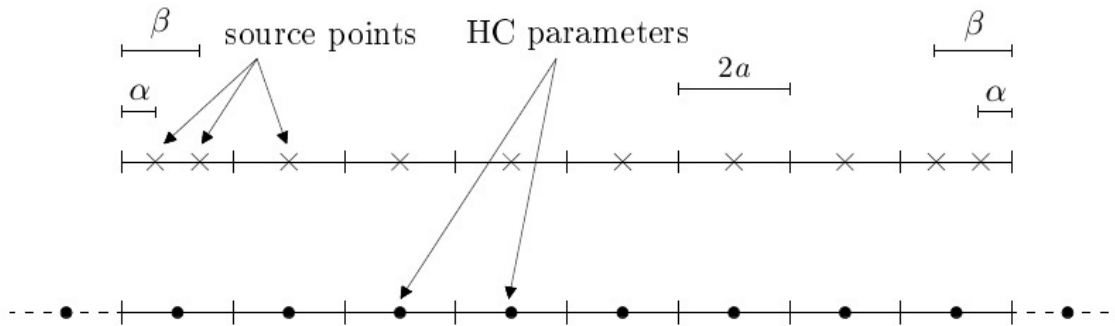


Figure 4: Arrangement of the source points on a macro-element.

In (14), the displacements and the tractions field  $\mathbf{u}$  and  $\mathbf{t}$  can be approximated by the following generic function

$$f_i(\zeta) = \sum_{k=1}^3 \phi^{(k)}(\zeta) f_i^{(k)} = \sum_{h=1}^3 \left( \sum_{h=0}^2 c_{hk}(\zeta^h) \right) f_i^{(k)} ; \quad i = 1 \dots n + 2 \quad (17)$$

where  $\zeta$  is the local element coordinate, with  $-1 < \zeta < 1$  (Figure 3.a),  $\phi^{(k)}(\zeta)$  is the interpolation function associated to the function  $f_i$  at node  $k$ , and  $c_{hk}$  is the coefficient of degree  $h$  of the polynomial corresponding to nodal parameter  $k$ . Also,  $n$  is the number of elements on a macro-element. For example, if there are  $n = 8$  elements (Figure 4), then we need 10 HC parameters.

The general expression of these functions is [55]

$$\begin{aligned} \phi^{(1)}(\zeta) &= \frac{1}{4(s+1)} (1 - 2\zeta + \zeta^2) \\ \phi^{(2)}(\zeta) &= \frac{1}{4(s+1)(d+1)} ((2 + 3(s+d) + 4sd) + 2(d-s)\zeta - (d+s+2)\zeta^2) \\ \phi^{(3)}(\zeta) &= \frac{1}{4(d+1)} (1 + 2\zeta + \zeta^2) \end{aligned} \quad (18)$$

where  $s = 1, d = 0$ , for the leftmost element in the macro-element,  $s = 0, d = 1$ , for the rightmost element, and  $s = 1, d = 1$ , for inside elements. In this work, the shape functions are generated using  $s = d = 1$  (inside element). Use of all three types of HC elements is onerous and it does not provide any advantage for the work carried out in this particular case, i.e., 2D plane orthotropic media. Therefore, we have

$$\begin{aligned} \phi^{(1)}(\zeta) &= \frac{1}{8} - \frac{1}{4}\zeta + \frac{1}{8}\zeta^2 \\ \phi^{(2)}(\zeta) &= \frac{3}{4} - \frac{1}{4}\zeta^2 \\ \phi^{(3)}(\zeta) &= \frac{1}{8} + \frac{1}{4}\zeta + \frac{1}{8}\zeta^2 \end{aligned} \quad (19)$$

## 2.4 Determination of the solution on the boundary

The discrete form of (14) allows to construct an algebraic system of equations in terms of contour variables. Using HC interpolation, the displacement and traction fields are represented inside each element by the following relations

$$\begin{aligned}\mathbf{u}(x) &= \phi_{ue} \mathbf{u}_e \\ \mathbf{t}(x) &= \phi_{te} \mathbf{t}_e\end{aligned}\quad (20)$$

with

$$\begin{aligned}\phi_e &= [\phi^{(j)} \quad \phi^{(j+1)} \quad \phi^{(j+2)}] \\ \mathbf{u}_e^T &= \begin{bmatrix} u_1^{(j)} & u_1^{(j+1)} & u_1^{(j+2)} \\ u_2^{(j)} & u_2^{(j+1)} & u_2^{(j+2)} \end{bmatrix} \\ \mathbf{t}_e^T &= \begin{bmatrix} t_1^{(j)} & t_1^{(j+1)} & t_1^{(j+2)} \\ t_2^{(j)} & t_2^{(j+1)} & t_2^{(j+2)} \end{bmatrix}\end{aligned}\quad (21)$$

where the generic terms  $\phi_e$  representing  $\phi_{ue}, \phi_{te}$ , are given by (19). In (21), the subscripts 1, 2, represent the field directions, and the superscripts  $j, j+1, j+2$  represent one of the three nodes involved in the interpolation for element  $e$ . Therefore, the discrete form of (14) becomes

$$\begin{aligned}\mathbf{c}^T \mathbf{u}(\xi) + \sum_{e=1}^{n_e} \int_{\Gamma_e} \mathbf{t}^{*T}(\xi, x) \phi_{ue} \mathbf{u}_e d\Gamma_e &= \\ &= \sum_{e=1}^{n_e} \int_{\Gamma_e} \mathbf{u}^{*T}(\xi, x) \phi_{te} \mathbf{t}_e d\Gamma_e + \sum_{c=1}^{n_c} \int_{\Omega_c} \mathbf{u}^{*T}(\xi, x) \mathbf{b}(x) d\Omega_c \quad (\xi \in \Gamma)\end{aligned}\quad (22)$$

where  $\xi$  denotes the position of the source,  $n_e$  the number of elements along the contour, and  $n_c$  is the number of cells in the domain. On the contour, arranging a number of sources equal to the number of parameters in the discretization, (22) becomes

$$\sum_e \mathbf{H}_e \mathbf{u}_e = \sum_e \mathbf{G}_e \mathbf{t}_e + \mathbf{b}\quad (23)$$

The contributions of element  $e$  to the matrices  $\mathbf{H}$  and  $\mathbf{G}$  are defined by

$$\begin{aligned}\mathbf{H}_e &= \int_{\Gamma_e} \mathbf{t}^{*T}(\xi, x) \phi_{ue} d\Gamma_e \\ \mathbf{G}_e &= \int_{\Gamma_e} \mathbf{u}^{*T}(\xi, x) \phi_{te} d\Gamma_e\end{aligned}\quad (24)$$

Using (23)–(24), the system (22) can be rewritten as follows

$$\mathbf{H}\mathbf{u} = \mathbf{G}\mathbf{t} + \mathbf{b}\quad (25)$$

Then, taking in account the boundary conditions of the problem, the system (25) can be rewritten in the compact form as

$$\mathbf{A}\mathbf{x} = \mathbf{f}\quad (26)$$

where the coefficient matrix  $\mathbf{A}$  contains both the coefficients of  $\mathbf{H}$ ,  $\mathbf{G}$ . The vector of unknowns  $\mathbf{x}$  collects the unknown values of the the displacement field  $\mathbf{u}$  and tractions  $\mathbf{t}$ . The vector  $\mathbf{f}$  is composed by the terms resulting from the product of the known values of  $\mathbf{u}$  and  $\mathbf{t}$  by the corresponding coefficients in the matrices  $\mathbf{H}$  and  $\mathbf{G}$ , plus the body forces  $\mathbf{b}$ , as it is explained next.

The boundary is composed of a collection of macro-elements that are subjected to either specified displacement or specified traction. For those macro-elements under specified displacement, the tractions are unknown, so in (26),  $\mathbf{A}$  receives values from  $\mathbf{G}$ , the unknowns  $\mathbf{x}$  are the tractions  $\mathbf{t}$ , and the RHS is calculated as  $\mathbf{f} = \mathbf{H}\mathbf{u} - \mathbf{b}$ . For the remaining macro-elements, which are subjected to specified traction, the displacements are unknown, so  $\mathbf{A}$  receives values from  $\mathbf{H}$ , the unknowns  $\mathbf{x}$  are the displacements  $\mathbf{u}$ , and the RHS is calculated as  $\mathbf{f} = \mathbf{G}\mathbf{t} + \mathbf{b}$ .

The size of matrix  $\mathbf{A}$  is very small when compared to the matrix of domain discretization methods (e.g., FEM), but it is full and not symmetric. Since  $\mathbf{x}$  includes both  $\mathbf{u}$  and  $\mathbf{t}$ , BEM is said to be *mixed*; that is, both displacements and tractions are evaluated simultaneously with comparable precision.

## 2.5 Analytical integration of boundary coefficients

The integrands in the boundary integrals (22) involve the products between the shape functions and the fundamental solutions (3) and (4). Analytical computation of these integrals is conveniently performed using a local coordinate system centered at the midpoint of the boundary element. The integrals have the following typical form

$$\int_{\Gamma} f^* \phi^{(k)}(x) d\Gamma = a \sum_{h=0}^2 c_{hk} \int_{-1}^1 f_i^* \zeta^{(h)} d\zeta \quad ; \quad i = 1 \dots n + 2 \quad (27)$$

where the abscissa  $\zeta = x/a$  is taken in a local system centered on the field element, and  $a$  indicates the half-length of the field element (Figure 5)). Note that  $i = 1 \dots n + 2$ , where  $n + 2$  is the number of parameters on a macro-element. For example, if there are  $n = 8$  elements (Figure 4), then we have 10 HC parameters.

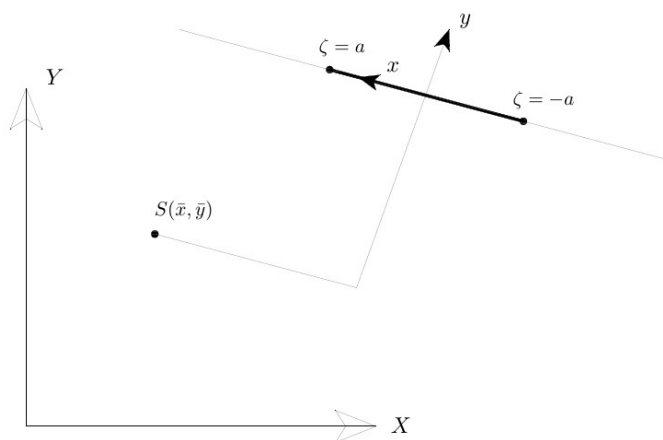


Figure 5: Coordinates of the source point  $S(\bar{x}, \bar{y})$  in the local system placed on the field element.

The integrals (27) have the following typical forms

$$\begin{aligned} E(k)_j^{(h)} &= \int_{\zeta_1}^{\zeta_2} \frac{\zeta^h}{(z_k^2)^j} d\zeta \\ G(k)_j^{(h)} &= \int_{\zeta_1}^{\zeta_2} \ln(z_k)(z_k^2)^j \zeta^h d\zeta \\ A(k)_j^{(h)} &= \int_{\zeta_1}^{\zeta_2} \arctan\left(\frac{\bar{y}}{\sqrt{\lambda_k}(\zeta - \bar{x})}\right) (z_k^2)^j \zeta^h d\zeta \end{aligned} \quad (28)$$

where  $\bar{x}, \bar{y}$  are the coordinates of the source point expressed in the local system of the field element and  $j$  is the power of the  $z_k^2$  term. The analytical solutions of the indefinite integrals  $E(k)_j^{(h)}$  can be written in the following recursive form

$$\begin{aligned} E(k)_j^{(h)} &= \frac{1}{2j - h - 1} \left\{ \left[ \frac{\zeta^{h-1}}{(z_k^2)^{j-1}} \right]_{\zeta_1}^{\zeta_2} + 2\bar{x}(j - h) E(k)_j^{(h-1)} + \right. \\ &\quad \left. + (h - 1) [(n_1 + n_2\lambda_k)\bar{x}^2 + (n_1\lambda_k + n_2)\bar{y}^2] E(k)_j^{(h-2)} \right\} \end{aligned} \quad (29)$$

When  $h = 2j - 1$ , it is necessary to use the following equation

$$E(k)_j^{(h)} = E(k)_{j-1}^{(h-2)} - [(n_1 + n_2\lambda_k)\bar{x}^2 + (n_1\lambda_k + n_2)\bar{y}^2] E(k)_j^{(h-2)} + 2\bar{x}E(k)_j^{(h-1)} \quad (30)$$

and, to initialize the recursive process when  $\bar{y} \neq 0$ , the following integrals are used

$$E(k)_1^{(0)} = \frac{1}{\sqrt{\lambda_k}\bar{y}} \left[ \arctan\left(\frac{(n_1 + n_2\sqrt{\lambda_k})(\zeta - \bar{x})}{(n_1\sqrt{\lambda_k} + n_2)\bar{y}}\right) \right]_{\zeta_1}^{\zeta_2} \quad (31a)$$

$$E(k)_1^{(1)} = \frac{1}{(n_1 + n_2\sqrt{\lambda_k})} \left[ \ln(z_k) \right]_{\zeta_1}^{\zeta_2} + \bar{x}E(k)_1^{(0)} \quad (31b)$$

$$E(k)_0^{(h)} = \left[ \frac{\zeta^{h+1}}{h+1} \right]_{\zeta_1}^{\zeta_2} \quad (31c)$$

$$E(k)_{j+1}^{(0)} = \frac{1}{2(n_1\lambda_k + n_2)\bar{y}^2 j} \left\{ \left[ \frac{(\zeta - \bar{x})}{(z_k^2)^j} \right]_{\zeta_1}^{\zeta_2} + (2j - 1) E(k)_j^{(0)} \right\} \quad (31d)$$

For  $\bar{y} = 0$  some of these expressions degenerate, and must be replaced by the following

$$E(k)_j^{(0)} = \left[ \frac{1}{(\zeta - \bar{x})^{2j-1}} \right]_{\zeta_1}^{\zeta_2} \frac{1}{(n_1 + n_2\lambda_k)(1 - 2j)} \quad (32)$$

Integrals of type  $G(k)_j^{(h)}$  can be represented in closed form. For the problem of 2D plane orthotropic media, only evaluation of integrals  $G(k)_0^{(h)}$  is required, which for  $\bar{y} \neq 0$  become

$$G(k)_0^{(h)} = \frac{1}{h+1} \left\{ \left[ \ln(z_k) \zeta^{h+1} \right]_{\zeta_1}^{\zeta_2} - (n_1 + n_2\lambda_k) \left( E(k)_1^{(h+2)} - \bar{x}E(k)_1^{(h+1)} \right) \right\} \quad (33)$$

When  $\bar{y} = 0$ , (33) becomes

$$G(k)_0^{(h)} = \frac{1}{h+1} \left\{ \left[ \zeta^h \left( (\zeta - \bar{x}) \ln(z_k) - \frac{\zeta}{h+1} \right) \right]_{\zeta_1}^{\zeta_2} + h\bar{x}G(k)_j^{(h-1)} \right\} \quad (34)$$

and the first integral of the recursive process is

$$G(k)_0^{(0)} = \left[ (\zeta - \bar{x}) \ln(z_k) - \zeta \right]_{\zeta_1}^{\zeta_2} \quad (35)$$

Also integrals of type  $A(k)_j^{(h)}$  can be represented in closed form. For the problem of 2D plane orthotropic media, only integrals  $A(k)_0^{(h)}$  are required

$$\begin{aligned} A(k)_0^{(h)} = & \\ & = \left[ -\frac{h}{h+1} \left( \frac{\bar{x}\bar{y}^{(h-1)}}{\sqrt{\lambda_k}} \right) + \frac{\bar{y}}{2\sqrt{\lambda_k}} \ln(z_k) \zeta^{(h)} + \frac{(h-1)}{6} \frac{\bar{y}^3}{\sqrt{\lambda_k^3}} \ln(z_k) + \right. \\ & \left. + \frac{h}{2} \frac{\bar{y}^2}{\lambda_k} \arctan \left( \frac{\sqrt{\lambda_k}(\zeta - \bar{x})}{\bar{y}} \right) \bar{x}^{(h-1)} - \arctan \left( \frac{\bar{y}}{\lambda_k(\zeta - \bar{x})} \right) \left( \frac{\zeta^{(h+1)} - \bar{x}^{(h+1)}}{h+1} \right) \right]_{\zeta_1}^{\zeta_2} \quad (36) \end{aligned}$$

and the first integral of the recursive process is

$$A(k)_0^{(0)} = \left[ \frac{\bar{y}}{2\sqrt{\lambda_k}} \ln(z_k) - \arctan \left( \frac{\bar{y}}{\lambda_k(\zeta - \bar{x})} \right) (\zeta - \bar{x}) \right]_{\zeta_1}^{\zeta_2} \quad (37)$$

Equations (27) to (37) allow us to evaluate the integrals in (22). After integration, the integrals  $\int_{\Gamma_e} \mathbf{u}^{*T} \phi_{te} d\Gamma_e$  and  $\int_{\Gamma_e} \mathbf{t}^{*T} \phi_{te} d\Gamma_e$  are expressed as combinations of  $E(k)_j^{(h)}$ ,  $A(k)_j^{(h)}$ , and  $G(k)_j^{(h)}$ , which are called  $U_{ij}^{(h)}$ , and  $T_{ij}^{(h)}$ , and reported in the Appendix. The expressions of  $U_{ij}^{(h)}$ ,  $T_{ij}^{(h)}$ , conveniently assembled, allow us to evaluate  $\mathbf{H}$  and  $\mathbf{G}$  in (25).

## 2.6 Domain solution

The solution in the interior of the domain can be obtained from the solution on the boundary. When the source point and the field point are very close ( $r_k \rightarrow 0$ ), the integrals of the form  $\int_{\Gamma} f^{*T}(\xi, x) g(x) d\Gamma$  become singular, so they are evaluated using Cauchy Principal Values (CPV) (see the Appendix (4)). Since there are no singularities in the domain,  $\mathbf{c} = \mathbb{I}$ ,<sup>2</sup> and using (14) we obtain

$$\mathbf{u}(\xi) = \int_{\Gamma} \mathbf{u}^{*T}(\xi, x) \mathbf{t}(x) d\Gamma - \int_{\Gamma} \mathbf{t}^{*T}(\xi, x) \mathbf{u}(x) d\Gamma + \int_{\Omega} \mathbf{u}^{*T}(\xi, x) \mathbf{b}(x) d\Omega \quad (\xi \in \Omega) \quad (38)$$

and in discrete form

$$\begin{aligned} \mathbf{u}(\xi) = & \\ = & \sum_{e=1}^{n_e} \int_{\Gamma_e} \mathbf{u}^{*T}(\xi, x) \phi_{te} \mathbf{t}_e d\Gamma_e - \sum_{e=1}^{n_e} \int_{\Gamma_e} \mathbf{t}^{*T}(\xi, x) \phi_{ue} \mathbf{u}_e d\Gamma_e + \sum_{c=1}^{n_c} \int_{\Omega_c} \mathbf{u}^{*T}(\xi, x) \mathbf{b}(x) d\Omega_c \quad (\xi \in \Omega) \end{aligned} \quad (39)$$

<sup>2</sup> $\mathbb{I}$ : Identity matrix.

Calculation of stress fields requires differentiation of the displacement field to obtain the strain field, as dictated by the kinematic equations [8, (1.4)], and further use of the constitutive equations [8, (1.55)], resulting in

$$\boldsymbol{\sigma}(\xi) = \int_{\Gamma} \mathbf{D}(\xi, x) \mathbf{t}(x) d\Gamma - \int_{\Gamma} \mathbf{S}(\xi, x) \mathbf{u}(x) d\Gamma + \int_{\Omega} \mathbf{D}(\xi, x) \mathbf{b}(x) d\Omega \quad (\xi \in \Omega) \quad (40)$$

and in discrete form

$$\boldsymbol{\sigma}(\xi) = \sum_{e=1}^{n_e} \int_{\Gamma_e} \mathbf{D} \phi_{te} \mathbf{t}_e d\Gamma_e - \sum_{e=1}^{n_e} \int_{\Gamma_e} \mathbf{S} \phi_{ue} \mathbf{u}_e d\Gamma_e + \sum_{c=1}^{n_c} \int_{\Omega_c} \mathbf{D} \mathbf{b}_c(x) d\Omega_c \quad (\xi \in \Omega) \quad (41)$$

where for 2D media

$$\mathbf{D}^T = \begin{bmatrix} D_{111} & D_{121} & D_{211} & D_{221} \\ D_{112} & D_{122} & D_{212} & D_{222} \end{bmatrix}; \quad \mathbf{S}^T = \begin{bmatrix} S_{111} & S_{121} & S_{211} & S_{221} \\ S_{112} & S_{122} & S_{212} & S_{222} \end{bmatrix} \quad (42)$$

and by analytic integration we obtain

$$\begin{aligned} D_{111} &= D \left( \sqrt{\lambda_2} A_1 \frac{r_1}{z_2^2} - \sqrt{\lambda_1} A_2 \frac{r_1}{z_1^2} \right) \\ D_{122} &= D \left( \lambda_1 \sqrt{\lambda_1} A_2 \frac{r_1}{z_1^2} - \lambda_2 \sqrt{\lambda_2} A_1 \frac{r_1}{z_2^2} \right) \\ D_{121} &= D \left( \sqrt{\lambda_2} A_1 \frac{r_2}{z_2^2} - \sqrt{\lambda_1} A_2 \frac{r_2}{z_1^2} \right) \\ D_{112} &= D_{121} \\ D_{211} &= D \left( \frac{A_2}{\sqrt{\lambda_2}} \frac{r_2}{z_2^2} - \frac{A_1}{\sqrt{\lambda_1}} \frac{r_2}{z_1^2} \right) \\ D_{222} &= D \left( \sqrt{\lambda_1} A_1 \frac{r_2}{z_1^2} - \sqrt{\lambda_2} A_2 \frac{r_2}{z_2^2} \right) \\ D_{212} &= D \left( \sqrt{\lambda_1} A_1 \frac{r_1}{z_1^2} - \sqrt{\lambda_2} A_2 \frac{r_1}{z_2^2} \right) \\ D_{212} &= D_{221} \end{aligned} \quad (43)$$

and

$$\begin{aligned} S_{111} &= D \left\{ \left[ \frac{1}{\sqrt{\lambda_2} z_2^2} - \frac{1}{\sqrt{\lambda_1} z_1^2} - 2 \left( \frac{\sqrt{\lambda_2} r_1^2}{z_2^4} - \frac{\sqrt{\lambda_1} r_1^2}{z_1^4} \right) \right] n_1 - 2 \left[ \frac{\sqrt{\lambda_2} r_1 r_2}{z_2^4} - \frac{\sqrt{\lambda_1} r_1 r_2}{z_1^4} \right] n_2 \right\} \\ S_{112} &= D \left\{ -2 \left[ \frac{\sqrt{\lambda_2} r_1 r_2}{z_2^4} - \frac{\sqrt{\lambda_1} r_1 r_2}{z_1^4} \right] n_1 + \left[ \frac{\sqrt{\lambda_2}}{z_2^2} - \frac{\sqrt{\lambda_1}}{z_1^2} - 2 \left( \frac{\sqrt{\lambda_2} r_2^2}{z_2^4} - \frac{\sqrt{\lambda_1} r_2^2}{z_1^4} \right) \right] n_2 \right\} \\ S_{121} &= S_{211} = S_{112} \\ S_{122} &= D \left\{ \left[ -\frac{\sqrt{\lambda_2}}{z_2^2} + \frac{\sqrt{\lambda_1}}{z_1^2} + 2 \left( \frac{\lambda_2 \sqrt{\lambda_2} r_1^2}{z_2^4} - \frac{\lambda_1 \sqrt{\lambda_1} r_1^2}{z_1^4} \right) \right] n_1 + 2 \left[ \frac{\lambda_2 \sqrt{\lambda_2} r_1 r_2}{z_2^4} - \frac{\lambda_1 \sqrt{\lambda_1} r_1 r_2}{z_1^4} \right] n_2 \right\} \\ S_{212} &= S_{221} = S_{122} \\ S_{222} &= D \left\{ 2 \left[ \frac{\lambda_2 \sqrt{\lambda_2} r_1 r_2}{z_2^4} - \frac{\lambda_1 \sqrt{\lambda_1} r_1 r_2}{z_1^4} \right] n_1 + \left[ -\frac{\lambda_2 \sqrt{\lambda_2}}{z_2^2} + \frac{\lambda_1 \sqrt{\lambda_1}}{z_1^2} + 2 \left( \frac{\lambda_2 \sqrt{\lambda_2} r_2^2}{z_2^4} - \frac{\lambda_1 \sqrt{\lambda_1} r_2^2}{z_1^4} \right) \right] n_2 \right\} \end{aligned} \quad (44)$$

Integral terms of the type  $D_{ijl}$  and  $S_{ijl}$ , written as functions of recurring integrals, are given in the Appendix.

The body force  $\mathbf{b}$  has been included for completeness, but no provisions have been made for its integration because we do not plan to use for our intended application (see Conclusions). Body force integration is a classical topic, where the goal is to avoid domain integration and use only boundary integration to guarantee all the advantages of BEM. Some classical papers describing techniques for transforming BEM domain integrals to the boundary are noted here [56–62].

### 3 Numerical Results

A number of cases are presented here to demonstrate the application of the proposed methodology to elastic analysis of 2-D orthotropic medium by the analytical integration of the kernels. The principal material directions are aligned with the Cartesian coordinate directions. All Abaqus simulations were performed using a uniform mesh of S8R elements. All elements had the same square shape. The reference values ( $U_{ref}$  or  $\sigma_{ref}$ ) used in the graphs have been evaluated numerically using a very fine mesh (i.e. values at convergence) employing Abaqus. A pointwise measure of the error has been used. The  $\log(|\cdot|)$  has been introduced to better emphasize the rate of convergence, where  $||$  denotes absolute value.

Please note that in the tabulated results one cannot measure the error by comparing BEM and FEM results between any pair of BEM and FEM discretizations, not even between the finer BEM and finer FEM meshes, because BEM and FEM meshes are not comparable. While a FEM mesh is a discretization of the domain, a BEM mesh is a discretization of the boundary. Therefore, identical results cannot be obtained. Only *convergence* and *rate of convergence* are meaningful, both of which are satisfied for both BEM and FEM, in all examples that follow.

#### 3.1 Square plate under uniform load

Consider an orthotropic square plate with side  $L = 100$  mm, subjected to uniformly distributed load  $q_y = 1.0$  N/mm along the principal material direction that coincides with the y-coordinate. Material properties are  $E_y = 161$  MPa,  $E_x = 90.27$  MPa,  $G_{xy} = 7.17$  MPa,  $\nu_{xy} = 0.28$  and thickness  $t = 1.2$  mm. The plate is clamped at  $x = 0$  loaded with  $q_y$  at  $y = L$  (Figure 6).

The results are compared with numerical results obtained using Abaqus. Comparison of the displacements at points A=( $L, 0$ ), B=( $L, L$ ), C=( $L/3, 2/3L$ ) and D=( $2/3L, L/3$ ) are presented in Tables 1 and 2. Both tables refer to the same degrees of freedom (dof) shown in Table 1.

Convergence of displacement at boundary points located in point A and B vs. number of degrees of freedom (dof) is depicted in Figure 7. It can be seen that BEM converges monotonically to the displacements using less dof than Abaqus. Convergence of displacement at domain point C vs. number of degrees of freedom (dof) is shown in Figure 8. It can be seen that BEM converges to the displacement using less dof than Abaqus.

Comparison of traction  $t_n$  at point E=( $0, L/2$ ) is shown in Table 3. Comparison of stresses at points C is presented in Table 4. The table refers to the same dof shown in Table 1. Convergence of stress at domain point C vs. number of degrees of freedom (dof) is shown in Figure 9. The BEM code shows a faster, monotonic convergence compared with Abaqus.

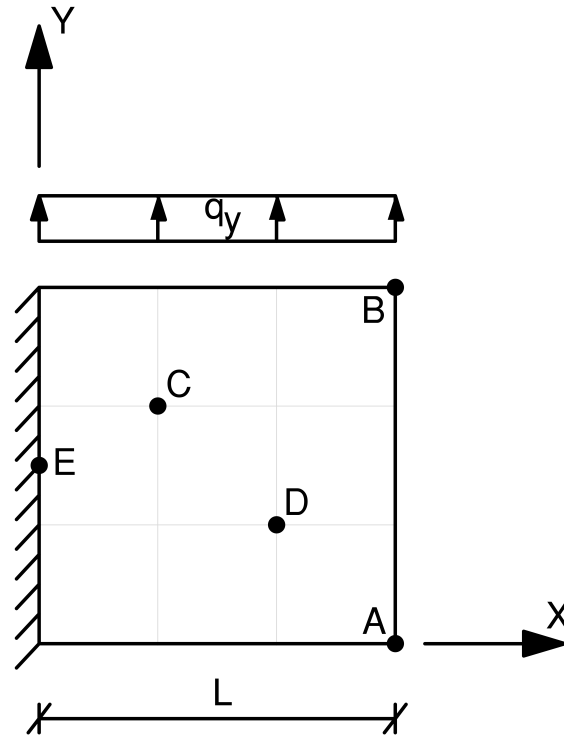


Figure 6: Square plate under uniform load.

Table 1: Comparison of displacements at points A and B, in [mm].

$N_{el}^{tot}$	<b>BEM</b>				$N_{el}^{tot}$	<b>Abaqus</b>			
	$L/N_{el}$	dof	$U_x^A$	$U_y^B$		$L/N_{el}$	dof	$U_x^A$	$U_y^B$
12	33.333	40	1.2216	8.3447	9	33.333	120	1.1671	6.9620
24	16.666	64	1.1908	8.2409	36	16.666	399	1.1447	7.6073
36	11.111	88	1.1895	8.2281	81	11.111	840	1.1507	7.8240
48	8.333	112	1.1773	8.2261	144	8.333	1443	1.1539	7.9279
60	6.666	136	1.1718	8.2258	225	6.666	2208	1.1557	7.9892
72	5.555	160	1.1690	8.2257	324	5.555	3135	1.1568	8.0296
84	4.761	184	1.1674	8.2257	441	4.761	4224	1.1575	8.0583
96	4.166	208	1.1665	8.2256	576	4.166	5475	1.1580	8.0796
108	3.703	232	1.1660	8.2254	729	3.703	6888	1.1584	8.0962
120	3.333	256	1.1657	8.2253	900	3.333	8463	1.1587	8.1094

Table 3: Convergence of normal traction  $t_n$  at point E.

$N_{el}^{tot}$	<b>BEM</b>	$t_n$	$N_{el}^{tot}$	<b>Abaqus</b>	$t_n$
12		0.012605	4		0.008728
20		0.019614	16		0.017994
132		0.019092	64		0.020206
220		0.019167	256		0.020206
308		0.019195	1024		0.019763
396		0.019208	4096		0.019122
484		0.019216	16384		0.019126

Table 2: Comparison of displacements at points C and D, in [mm].

<b>BEM</b>				<b>Abaqus</b>			
$U_x^C$	$U_y^C$	$U_x^D$	$U_y^D$	$U_x^C$	$U_y^C$	$U_x^D$	$U_y^D$
-0.1353	3.8428	0.1546	6.5786	-0.0244	2.1964	0.1167	5.2396
-0.1234	3.7846	0.1410	6.4863	-0.1158	3.2045	0.1373	5.8530
-0.1220	3.7726	0.1388	6.5539	-0.1150	3.3630	0.1377	6.0612
-0.1214	3.7680	0.1380	6.4607	-0.1167	3.4707	0.1373	6.1623
-0.1211	3.7657	0.1376	6.4575	-0.1179	3.5285	0.1371	6.2225
-0.1209	3.7644	0.1374	6.4556	-0.1184	3.5678	0.1370	6.2622
-0.1208	3.7636	0.1373	6.4545	-0.1189	3.5955	0.1369	6.2904
-0.1207	3.7631	0.1372	6.4537	-0.1192	3.6162	0.1369	6.3115
-0.1206	3.7627	0.1371	6.4532	-0.1194	3.6323	0.1368	6.3279
-0.1206	3.7624	0.1371	6.4528	-0.1196	3.6451	0.1368	6.3409

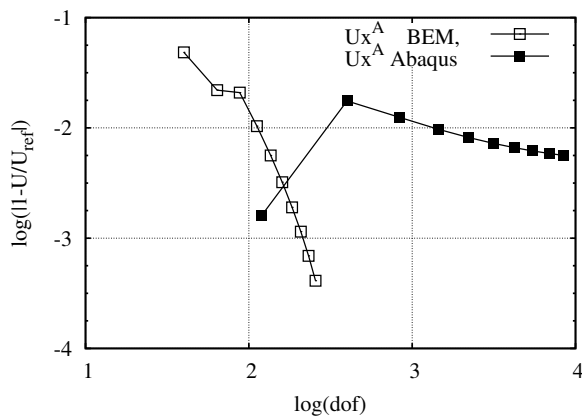
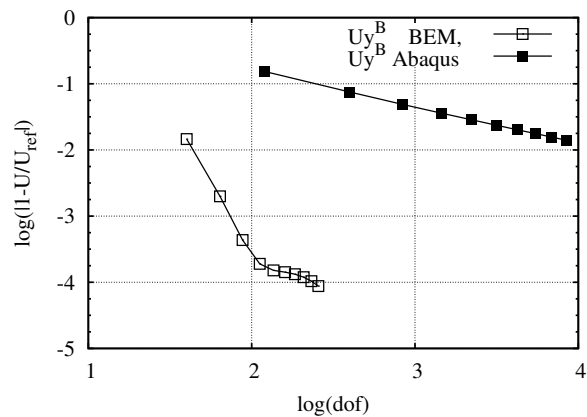
(a)  $U_x^A$ (b)  $U_y^B$ 

Figure 7: Convergence of displacement at boundary points A and B vs. degrees of freedom (dof).

Table 4: Comparison of stresses at point C, in [MPa].

BEM			Abaqus		
$\sigma_{xx}^C$	$\sigma_{yy}^C$	$\tau_{xy}^C$	$\sigma_{xx}^C$	$\sigma_{yy}^C$	$\tau_{xy}^C$
0.54971	-0.67136	-0.25424	0.30868	-0.93328	-0.12980
0.54617	-0.66513	-0.24929	0.60545	-0.60281	-0.18117
0.54546	-0.66450	-0.24457	0.53595	-0.68128	-0.23643
0.54515	-0.66417	-0.24264	0.54351	-0.66386	-0.23595
0.54508	-0.66413	-0.24225	0.54446	-0.66640	-0.23756
0.54504	-0.66411	-0.24200	0.54368	-0.66524	-0.23886
0.54502	-0.66409	-0.24183	0.54388	-0.66528	-0.23943
0.54500	-0.66409	-0.24170	0.54388	-0.66510	-0.23984
0.54500	-0.66409	-0.24161	0.54390	-0.66504	-0.24013
0.54498	-0.66408	-0.24150	0.54393	-0.66498	-0.24034

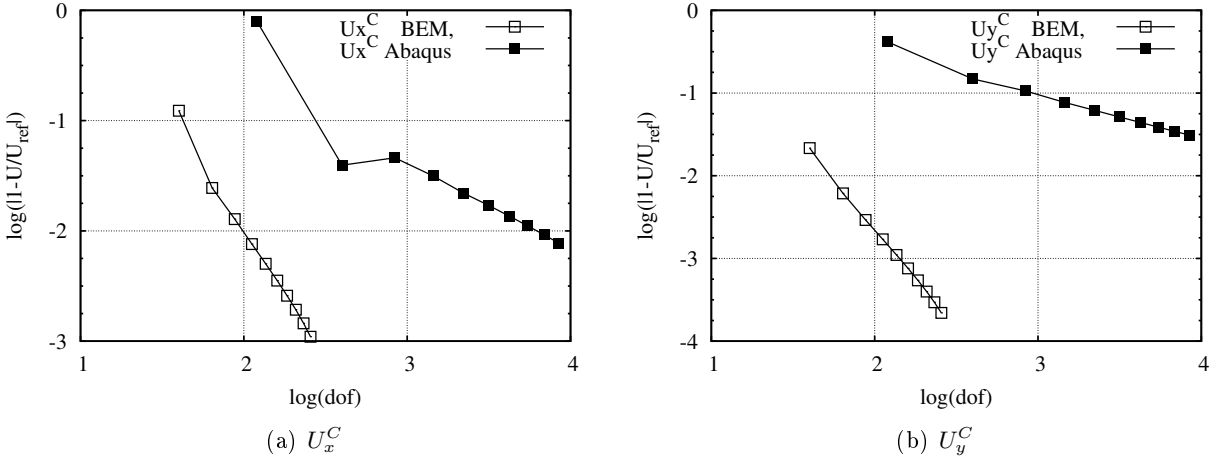


Figure 8: Convergence of displacement at domain point C vs. degrees of freedom (dof).

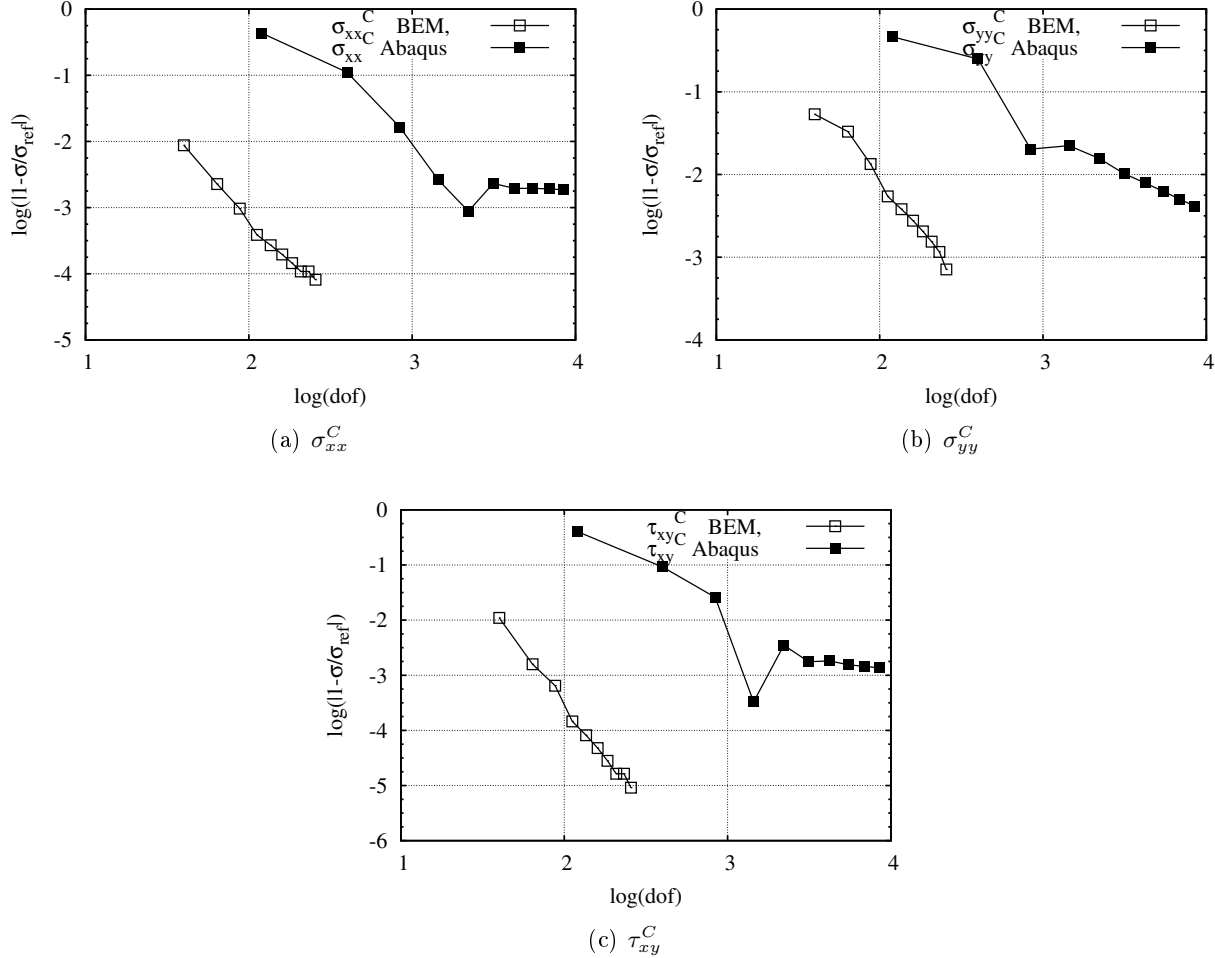


Figure 9: Convergence of stress at domain point C vs. degrees of freedom (dof).

### 3.2 Cantilever plate under uniform shear load

Consider an orthotropic cantilever plate with base  $b = 200$  mm (along  $x$ ) and height  $h = 10$  mm (along  $y$ ), subjected to uniformly distributed shear load  $q_y = -0.030$  N/mm at  $x = b$ . The plate is clamped at  $x = 0$ . The principal material direction coincides with the  $x$ -coordinate. Material properties are  $E_x = 85$  MPa,  $E_y = 74$  MPa,  $G_{xy} = 10$  MPa,  $\nu_{xy} = 0.3$  and thickness  $t = 1$  mm. For optimum accuracy, the length of the elements are constant for all macro-elements.

A typical mesh is shown in Figure 10. The element size is shown as  $h/N_{el}$  in Table 5.



Figure 10: Typical mesh used for Abaqus discretization. Cantilever plate under uniform shear load.

The results are compared with numerical results obtained using Abaqus at points  $A=(b,0)$ ,  $B=(b,h)$ ,  $C=(0, h/2)$ , and  $D=(b/5, h/2)$ . Comparison of displacements at points A and B are presented in Table 5. Convergence of displacement at boundary points A and B vs. number of degrees of freedom (dof) is shown in Figure 11. It can be seen that BEM shows an higher rate of convergence than Abaqus.

Convergence of stress at domain point D vs. degrees of freedom (dof) is reported in Table 6 and Figure 12, while tangential traction  $t_t$  at point C in Table 7 and Figure 12. It can be seen that BEM converges to the traction/stress using less dof than Abaqus.

Table 5: Comparison of displacements at points A and B, in [mm].

$N_{el}^{tot}$	$h/N_{el}$	BEM			Abaqus				
		dof	$U_y^A$	$U_x^B$	$N_{el}^{tot}$	$h/N_{el}$	dof	$U_y^A$	$U_x^B$
42	10	100	-111.2293	4.1389	20	10	309	-113.1230	4.2252
84	5	184	-111.3818	4.1535	80	5	975	-113.2740	4.2290
168	2.5	352	-112.1102	4.1825	320	2.5	3387	-113.4370	4.2333
336	1.25	688	-112.8399	4.2085	1280	1.25	12531	-113.5280	4.2358
672	0.625	1360	-113.1830	4.2206	5120	0.625	48099	-113.6040	4.2378
1344	0.3125	2704	-113.3130	4.2252					

Table 6: Comparison of stress  $\tau_{xy}$  [MPa] at point D.

BEM				Abaqus			
$N_{el}^{tot}$	$h/N_{el}$	dof	$\tau_{xy}^D$	$N_{el}^{tot}$	$h/N_{el}$	dof	$\tau_{xy}^D$
42	10	100	-0.04490	20	10	309	-0.02926
84	5	184	-0.04400	80	5	975	-0.05265
168	2.5	352	-0.04438	320	2.5	3387	-0.04687
336	1.25	688	-0.04493	1280	1.25	12531	-0.04546
672	0.625	1360	-0.04520	5120	0.625	48099	-0.04511
1344	0.3125	2704	-0.04530				

Table 7: Comparison of tangential traction  $t_t$  at point C.

BEM				Abaqus			
$N_{el}^{tot}$	$h/N_{el}$	dof	$t_t^C$	$N_{el}^{tot}$	$h/N_{el}$	dof	$t_t^C$
42	10	100	0.4739	20	10	309	0.0194
126	3.333	268	0.1245	80	5	975	0.0105
210	2	436	0.1237	320	2.5	3387	0.0043
462	0.909	940	0.1125	1280	1.25	12531	0.0022
714	0.588	1444	0.1112	5120	0.625	48099	0.1047
1470	0.285	2956	0.1105				

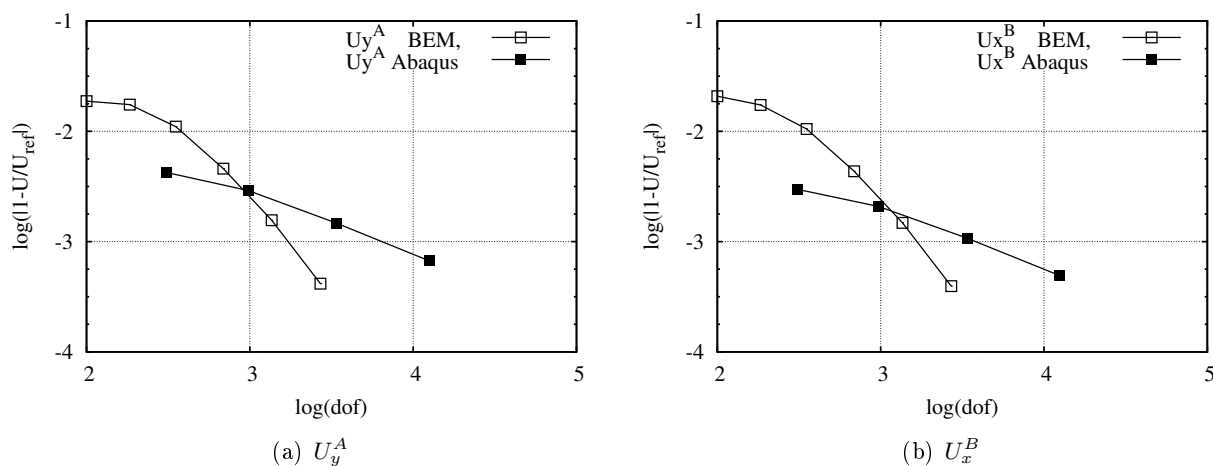


Figure 11: Convergence of displacement at boundary points A and B vs. number of degrees of freedom (dof).

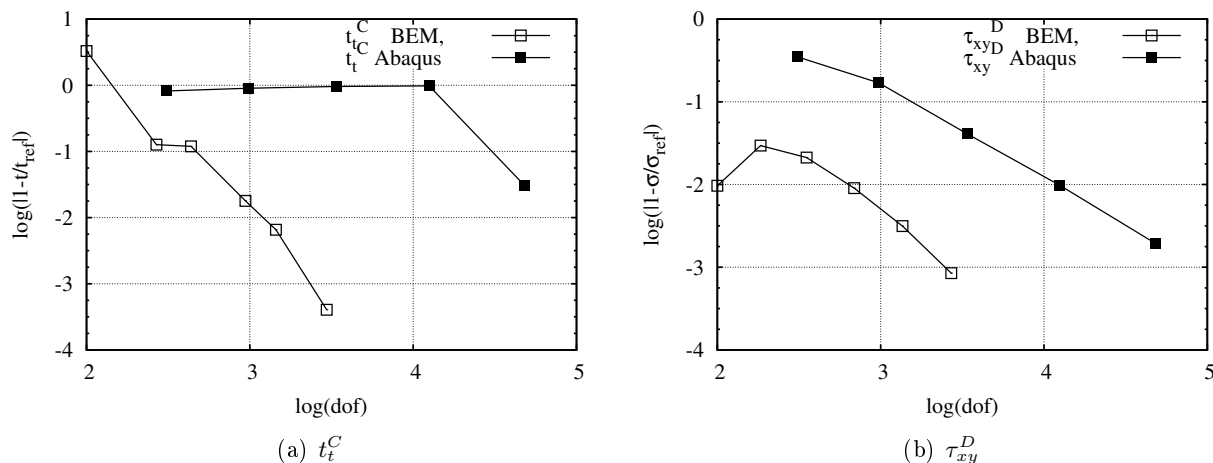


Figure 12: Convergence of tangential traction at point C and stress at domain point D vs. number of degrees of freedom (dof).

### 3.3 L-shape plate under uniform shear load

Consider an orthotropic irregular plate subjected to a uniformly distributed shear load  $q_y = -0.0135$  N/mm along the principal material direction that coincides with the  $y$ -coordinate (Figure 13). Material properties are  $E_y = 85$  MPa,  $E_x = 74$  MPa,  $G_{xy} = 20$  MPa,  $\nu_{xy} = 0.3$ . The length is  $L = 100$  mm and thickness  $t = 1.3$  mm. Element size is uniform along the boundary, and given as  $L/N_{el}$  in Table 8 for each level of discretization.

The results are compared at four points. The first three points,  $A=(2.5L, 1.5L)$ ,  $B=(2.5L, 2.5L)$  and  $C=(L, L)$  are located on the boundary. The point  $D=(1.5L, 2.0L)$  is located in the domain.

Convergence of displacement at boundary points located in point A and B vs. number of degrees of freedom (dof) is shown in Table 8 and Figure 14. It can be seen that BEM converges monotonically to the displacement solution using less dof than Abaqus. Convergence of displacement at point C vs. number of degrees of freedom (dof) is shown in Table 9 and Figure 15. It can be seen that BEM converges to the displacement using less dof than Abaqus.

Convergence of stress at domain point D vs. number of degrees of freedom (dof) is reported in Table 10 and Figure 16. The BEM code shows faster, monotonic convergence compared with Abaqus.

Figure 13: L-shape plate under uniform shear load.

Table 8: Comparison of displacements at points A and B, in [mm].

$N_{el}^{tot}$	$L/N_{el}$	<b>BEM</b>			<b>Abaqus</b>				
		dof	$U_x^B$	$U_y^A$	$N_{el}^{tot}$	$L/N_{el}$	dof	$U_x^B$	$U_y^A$
20	50	64	1.0646	-1.5967	16	50	207	1.0382	-1.4912
40	25	104	1.0777	-1.6052	64	25	699	1.0601	-1.5475
80	12.5	184	1.0801	-1.6032	256	12.5	2547	1.0709	-1.5748
160	6.25	344	1.0807	-1.6014	1024	6.25	9699	1.0759	-1.5873
320	3.125	664	1.0808	-1.6003	4096	3.125	37827	1.0781	-1.5931

Table 9: Comparison of displacements at point C, in [mm].

$N_{el}^{tot}$	$L/N_{el}$	<b>BEM</b>			<b>Abaqus</b>				
		dof	$U_x^C$	$U_y^C$	$N_{el}^{tot}$	$L/N_{el}$	dof	$U_x^C$	$U_y^C$
20	50	64	0.2752	-0.2822	16	50	207	0.3241	-0.2598
40	25	104	0.3155	-0.2381	64	25	699	0.3167	-0.2605
80	12.5	184	0.3112	-0.2419	256	12.5	2547	0.3113	-0.2593
160	6.25	344	0.3078	-0.2446	1024	6.25	9699	0.3075	-0.2574
320	3.125	664	0.3052	-0.2465	4096	3.125	37827	0.3048	-0.2557

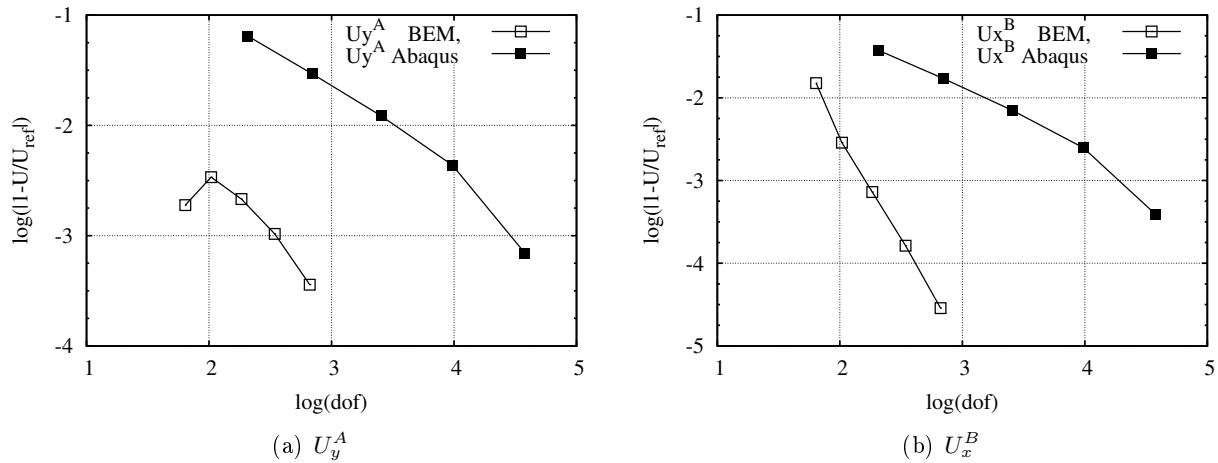


Figure 14: Convergence of displacement at boundary points A and B vs. number of degrees of freedom (dof).

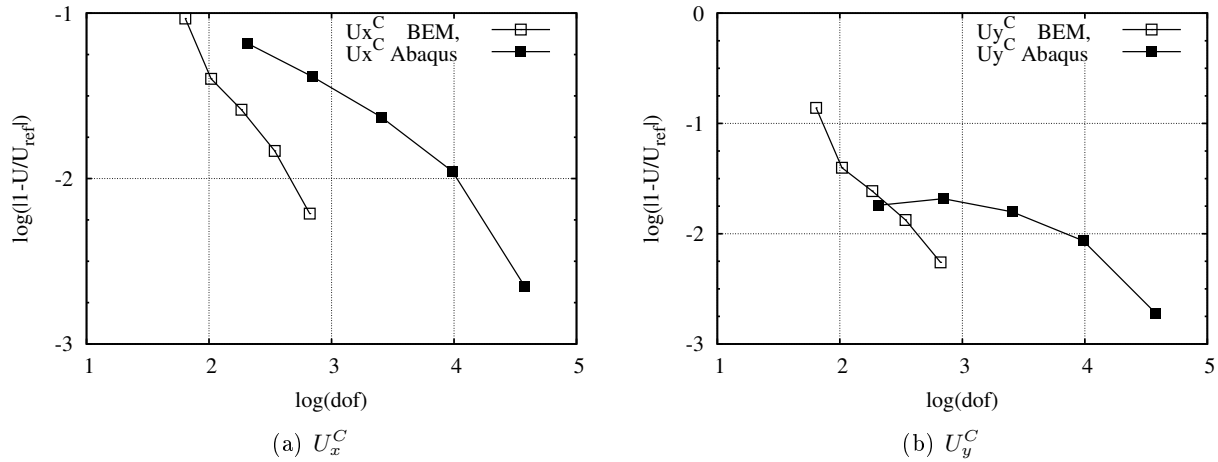


Figure 15: Convergence of displacement at boundary point C vs. number of degrees of freedom (dof).

Table 10: Comparison of stress at point D, in [MPa].

$N_{el}^{tot}$	$L/N_{el}$	BEM			Abaqus				
		dof	$\sigma_{xx}^D$	$\tau_{xy}^D$	$N_{el}^{tot}$	$L/N_{el}$	dof	$\sigma_{xx}^D$	$\tau_{xy}^D$
20	50	64	-0.00058	0.01520	16	50	207	-0.00786	0.02247
40	25	104	-0.00122	0.01528	64	25	699	-0.00185	0.01563
80	12.5	184	-0.00137	0.01524	256	12.5	2547	-0.00171	0.01525
160	6.25	344	-0.00143	0.01522	1024	6.25	9699	-0.00160	0.01519
320	3.125	664	-0.00146	0.01521	4096	3.125	37827	-0.00155	0.01518

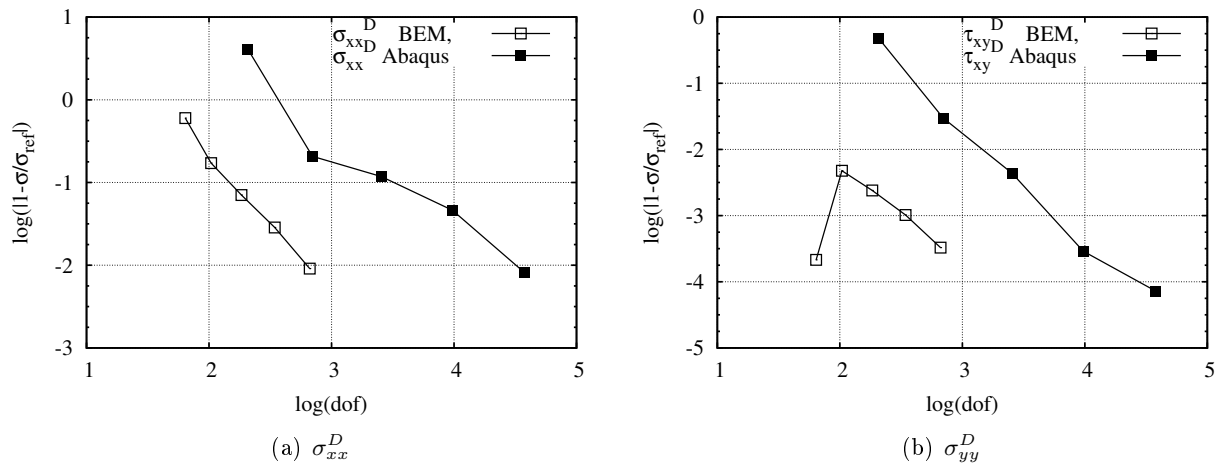


Figure 16: Convergence of stress at domain point D vs. number of degrees of freedom (dof).

### 3.4 Laminated plate under shear load

Consider a laminated rectangular plate with base  $b = 200$  mm (along  $x$ ) and height  $h = 100$  mm (along  $y$ ), subjected to uniformly distributed shear load  $q_y = -0.24$  N/mm at  $x = b$ . The plate is clamped at  $x = 0$ . The laminate has 5 lamina, arranged in a  $[90/-90/0/-90/90]$  configuration. The thickness of each lamina is  $t = 0.3$  mm. The laminated plate is modeled using its equivalent orthotropic properties [2, §6.4, Eq. (6.4)], i.e.,  $E_x = 120$  MPa,  $E_y = 60$  MPa,  $G_{xy} = 7$  MPa,  $\nu_{xy} = 0.071$ . A typical mesh is shown in Figure 17. The element size is shown as  $h/N_{el}$  in Table 11.

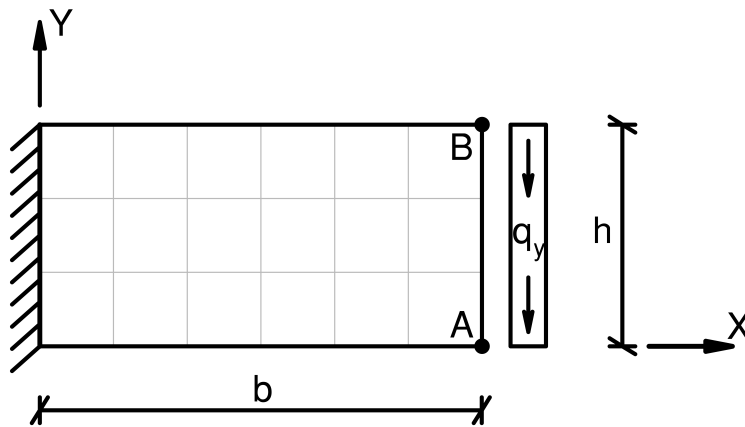


Figure 17: Typical mesh used for Abaqus discretization. Laminated plate under shear load.

The results are compared with numerical results obtained using Abaqus at points  $A=(b,0)$ , and  $B=(b,h)$ . Comparison of displacements at points A and B is shown in Table 11. Convergence of displacement at boundary points located at points A and B vs. degrees of freedom (dof) is shown in Figure 18. It can be seen that BEM converges to the displacements using less dof than Abaqus.

Table 11: Comparison of displacements at points A and B, in [mm].

$N_{el}^{tot}$	$b/N_{el}$	BEM			Abaqus				
		dof	$U_x^A$	$U_y^B$	$N_{el}^{tot}$	$b/N_{el}$	dof	$U_x^A$	$U_y^B$
18	33.333	52	2.8786	12.5133	18	33.333	219	2.9083	12.2900
36	16.666	88	2.9099	12.5220	72	16.666	759	2.9284	12.4542
72	8.3333	160	2.9273	12.5436	288	8.3333	2811	2.9393	12.5254
144	4.1666	304	2.9354	12.5553	1152	4.1666	10803	2.9445	12.5584
288	2.0833	592	2.9392	12.5604	4608	2.0833	42339	2.9470	12.5746
576	1.0416	1168	2.9411	12.5626	18432	1.0416	167619	2.9482	12.5826

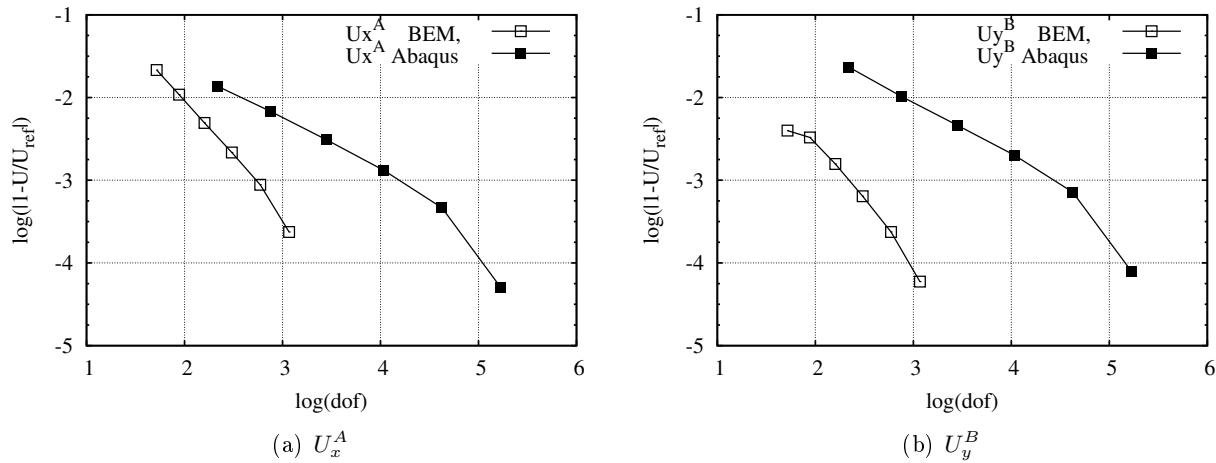


Figure 18: Convergence of displacement at boundary points A and B vs. number of degrees of freedom (dof).

## 4 Conclusions

The main contributions of this work are the analytical integration of singular kernels for plane orthotropic media, and a successful implementation into a BEM code. Numerical examples show that the results obtained by the proposed BEM implementation are in good agreement with those obtained by FEM, demonstrating the validity and reliability of the proposed BEM formulation for the analysis of elastic, 2D, orthotropic media. The analytical evaluation of the integral coefficients and the efficiency of the implementation is highlighted. All equations are analytically integrated and expressed as a function of a few recurring integrals, contributed for the first time in this work. The analytically integrated, HC interpolated BEM formulation converges much faster than a displacement-based FEM, for both displacements and stresses. Stresses always converge monotonically, while FEM sometimes displays oscillatory, slow convergence. The proposed model is able to represent stress concentrations well. HC interpolation allows  $C^1$  continuity with negligible increment of dof with respect to piecewise constant interpolation. The BEM formulation is mixed, providing displacements and tractions simultaneously and with the same order of approximation, which is significant for stress analysis. Further, the dimensionality of the model is reduced by one (from 2D to 1D), which coupled with analytical integration and efficient interpolation leads to fast convergence

and economical solution with fewer dof than required by FEM.

The proposed BEM formulation can be used to solve a variety of problems involving orthotropic media. In the future, we wish to solve an orthotropic representative volume element that is the micro-model of a micro/macro model. Since the micro model must be solved for each Gauss point at each iteration of the (nonlinear) macro model, computational cost is critical. The proposed formulation is clearly more economical than a FEM micro-model. Our intended applications is for a flat panel. Therefore, we did not study the applicability and performance of the proposed method to solve problems with curved geometries. Furthermore, our proposed application does not include body forces.

## Appendix

### Coefficients $U_{ij}^{(h)}$ and $T_{ij}^{(h)}$

Coefficients  $U_{ij}^{(h)}, T_{ij}^{(h)}$  are given next:

$$U_{11}^{(h)} = D \left[ \sqrt{\lambda_1} A_2^2 G(1)_0^{(h)} - \sqrt{\lambda_2} A_1^2 G(2)_0^{(h)} \right] \quad (45a)$$

$$U_{12}^{(h)} = DA_1 A_2 \left[ A(2)_0^{(h)} - A(1)_0^{(h)} \right] \quad (45b)$$

$$U_{21}^{(h)} = U_{12}^{(h)} \quad (45c)$$

$$U_{22}^{(h)} = -D \left[ \frac{A_1^2}{\sqrt{\lambda_1}} G(1)_0^{(h)} - \frac{A_2^2}{\sqrt{\lambda_2}} G(2)_0^{(h)} \right] \quad (45d)$$

For  $n_1 = 0$  and  $n_2 = 1$

$$T_{11}^{(h)} = \bar{y}D \left[ \sqrt{\lambda_2} A_1 E(2)_1^{(h)} - \sqrt{\lambda_1} A_2 E(1)_1^{(h)} \right] \quad (46a)$$

$$T_{12}^{(h)} = D \left[ \sqrt{\lambda_1} A_1 \tilde{E}(1)_1^{(h)} - \sqrt{\lambda_2} A_2 \tilde{E}(2)_1^{(h)} \right] \quad (46b)$$

$$T_{21}^{(h)} = D \left[ \lambda_1 \sqrt{\lambda_1} A_2 \tilde{E}(1)_1^{(h)} - \lambda_2 \sqrt{\lambda_2} A_1 \tilde{E}(2)_1^{(h)} \right] \quad (46c)$$

$$T_{22}^{(h)} = \bar{y}D \left[ \sqrt{\lambda_1} A_1 E(1)_1^{(h)} - \sqrt{\lambda_2} A_2 E(2)_1^{(h)} \right] \quad (46d)$$

For  $n_1 = 1$  and  $n_2 = 0$

$$T_{11}^{(h)} = \bar{y}D \left[ \sqrt{\lambda_2} A_1 E(2)_1^{(h)} - \sqrt{\lambda_1} A_2 E(1)_1^{(h)} \right] \quad (47a)$$

$$T_{12}^{(h)} = D \left[ \frac{A_1}{\sqrt{\lambda_1}} \tilde{E}(1)_1^{(h)} - \frac{A_2}{\sqrt{\lambda_2}} \tilde{E}(2)_1^{(h)} \right] \quad (47b)$$

$$T_{21}^{(h)} = D \left[ \sqrt{\lambda_1} A_2 \tilde{E}(1)_1^{(h)} - \sqrt{\lambda_2} A_1 \tilde{E}(2)_1^{(h)} \right] \quad (47c)$$

$$T_{22}^{(h)} = \bar{y}D \left[ \sqrt{\lambda_1} A_1 E(1)_1^{(h)} - \sqrt{\lambda_2} A_2 E(2)_1^{(h)} \right] \quad (47d)$$

where

$$\tilde{E}(k)_j^{(h)} = E(k)_j^{(h+1)} - \bar{x}E(k)_j^{(h)} \quad (48)$$

and  $n$  is the unit outward normal to the boundary took in the global reference system  $X, Y$ , so  $n_1 = n_x$  and  $n_2 = n_y$ .

### Coefficients $D_{ijl}^{(h)}$ and $S_{ijl}^{(h)}$

Integral terms of the type  $D_{ijl}^{(h)}$  shown in (43), written as function of the recurring integrals, have the following form

$$D_{111}^{(h)} = D \left[ \sqrt{\lambda_2} A_1 \tilde{E}(2)_1^{(h)} - \sqrt{\lambda_1} A_2 \tilde{E}(1)_1^{(h)} \right] \quad (49a)$$

$$D_{122}^{(h)} = D \left[ \lambda_1 \sqrt{\lambda_1} A_2 \tilde{E}(1)_1^{(h)} - \lambda_2 \sqrt{\lambda_2} A_1 \tilde{E}(2)_1^{(h)} \right] \quad (49b)$$

$$D_{121}^{(h)} = \bar{y} D \left[ \sqrt{\lambda_2} A_1 E(2)_1^{(h)} - \sqrt{\lambda_1} A_2 E(1)_1^{(h)} \right] \quad (49c)$$

$$D_{112}^{(h)} = D_{121}^{(h)} \quad (49d)$$

$$D_{211}^{(h)} = \bar{y} D \left[ \frac{A_2}{\sqrt{\lambda_2}} E(2)_1^{(h)} - \frac{A_1}{\sqrt{\lambda_1}} E(1)_1^{(h)} \right] \quad (49e)$$

$$D_{222}^{(h)} = \bar{y} D \left[ \sqrt{\lambda_1} A_1 E(1)_1^{(h)} - \sqrt{\lambda_2} A_2 E(2)_1^{(h)} \right] \quad (49f)$$

$$D_{212}^{(h)} = D \left[ \sqrt{\lambda_1} A_1 \tilde{E}(1)_1^{(h)} - \sqrt{\lambda_2} A_2 \tilde{E}(2)_1^{(h)} \right] \quad (49g)$$

$$D_{212}^{(h)} = D_{221}^{(h)} \quad (49h)$$

and integrals of the type  $S_{ijl}^{(h)}$  shown in (44), can be written for  $n_1 = 0$  and  $n_2 = 1$  as

$$S_{111}^{(h)} = -2\bar{y} D \left[ \sqrt{\lambda_2} \tilde{E}(2)_2^{(h)} - \sqrt{\lambda_1} \tilde{E}(1)_2^{(h)} \right] \quad (50a)$$

$$S_{112}^{(h)} = D \left[ \sqrt{\lambda_2} E(2)_1^{(h)} - \sqrt{\lambda_1} E(1)_1^{(h)} - 2\bar{y}^2 \left( \lambda_2 E(2)_2^{(h)} - \lambda_1 E(2)_1^{(h)} \right) \right] \quad (50b)$$

$$S_{121}^{(h)} = S_{211}^{(h)} = S_{112}^{(h)} \quad (50c)$$

$$S_{122}^{(h)} = 2\bar{y} D \left[ \lambda_2 \sqrt{\lambda_2} \tilde{E}(2)_2^{(h)} - \lambda_1 \sqrt{\lambda_1} \tilde{E}(1)_2^{(h)} \right] \quad (50d)$$

$$S_{212}^{(h)} = S_{221}^{(h)} = S_{122}^{(h)} \quad (50e)$$

$$S_{222}^{(h)} = D \left[ \lambda_1 \sqrt{\lambda_1} \tilde{E}(1)_1^{(h)} - \lambda_2 \sqrt{\lambda_2} \tilde{E}(2)_1^{(h)} + 2\bar{y}^2 \left( \lambda_2 \sqrt{\lambda_2} E(2)_2^{(h)} - \lambda_1 \sqrt{\lambda_1} E(2)_1^{(h)} \right) \right] \quad (50f)$$

and for  $n_1 = 1$  and  $n_2 = 0$ , as

$$S_{111}^{(h)} = D \left[ \frac{1}{\sqrt{\lambda_2}} E(2)_1^{(h)} - \frac{1}{\sqrt{\lambda_1}} E(1)_1^{(h)} - 2\bar{y}^2 \left( \sqrt{\lambda_2} E(2)_2^{(h)} - \sqrt{\lambda_1} E(1)_2^{(h)} \right) \right] \quad (51a)$$

$$S_{112}^{(h)} = -2\bar{y}D \left[ \sqrt{\lambda_2} \tilde{E}(2)_2^{(h)} - \sqrt{\lambda_1} \tilde{E}(1)_2^{(h)} \right] \quad (51b)$$

$$S_{121}^{(h)} = S_{211}^{(h)} = S_{112}^{(h)} \quad (51c)$$

$$S_{122}^{(h)} = D \left[ \sqrt{\lambda_1} E(1)_1^{(h)} - \sqrt{\lambda_2} E(2)_1^{(h)} + 2\bar{y}^2 \left( \lambda_2 \sqrt{\lambda_2} E(2)_2^{(h)} - \lambda_1 \sqrt{\lambda_1} E(1)_2^{(h)} \right) \right] \quad (51d)$$

$$S_{212}^{(h)} = S_{221}^{(h)} = S_{122}^{(h)} \quad (51e)$$

$$S_{222}^{(h)} = 2\bar{y}D \left[ \lambda_2 \sqrt{\lambda_2} \tilde{E}(2)_2^{(h)} - \lambda_1 \sqrt{\lambda_1} \tilde{E}(1)_2^{(h)} \right] \quad (51f)$$

with  $r_k, \lambda_1, \lambda_2, A_k, z_k$ , and  $D$  given in (5)–(10).

### Singular and near singular integrals

The calculation of the integrals on the boundary (14) brings to some integration problems, absent in the calculation of them in the domain. When the source point  $\xi$  is coincident with the field point  $x$ , the kernels of the integrals show some singularities.

The kernel function  $u^*(\xi, x)$  have two weak singularities,  $O(\ln z_k)$  and  $O(\arctan(r_2/\sqrt{\lambda_k}r_1))$ . The kernel function  $t^*(\xi, x)$  has a strong singularity  $O(1/z_k^2)$  [63].

The weak singularities disappear when we integrate the integrals on the boundary. The strong singularity requires the evaluation of the integrals as as Cauchy Principal Value (CPV). The evaluation of Cauchy Principal Value (CPV) integrals is one of the typical aspects of the Boundary Element Method (BEM). It is essentially due to the strong singularity shown by some kernel functions appearing in some boundary integral equations.

In this Appendix, the distance between source and field point  $r_k$  is denoted with  $\varepsilon$  to emphasize that it is an infinitesimal quantity.

### Integration of kernels with singularity $O(1/z_k^2)$

#### Integration of $t_{11}$ and $t_{22}$

From the integral equation (14) consider the kernel function  $t_{ij}$ . When the distance between the source point  $\xi$  and the field point  $x$  tends to 0,  $\varepsilon \rightarrow 0$ , the integration of kernel  $t_{ij}$  shows a strong singularity that necessitates evaluation of the integral as CPV.

Figure 19: Singular part of  $t_{11}^*$ .

We illustrate the integration procedure using  $t_{11}$ . The integration of  $t_{22}$  follows the same procedure. Let's consider

$$\int_{\Gamma} t_{11}^{*T} u \, d\Gamma = \lim_{\varepsilon \rightarrow 0} \left[ \underbrace{\int_{\Gamma - \Gamma_{\varepsilon}} t_{11}^{*T} u \, d(\Gamma - \Gamma_{\varepsilon})}_{I_A} + \underbrace{\int_{\Gamma_{\varepsilon}} t_{11}^{*T} u \, d\Gamma_{\varepsilon}}_{I_B} \right]$$

where  $\varepsilon$  is distance between the source and field point, where

$$I_A = \lim_{\varepsilon \rightarrow 0} \int_{\Gamma - \Gamma_{\varepsilon}} t_{11}^{*T} u \, d(\Gamma - \Gamma_{\varepsilon}) = \int_{\Gamma} t_{11}^{*T} u \, d\Gamma$$

The term  $I_A$  is part of the system (14), on the right side. This term has no singular contribution because it is far from the semi-circle in Fig (19). Next,

$$I_B = \int_{\Gamma_{\varepsilon}} t_{11}^{*T} u \, d\Gamma_{\varepsilon} = I_{B1} + I_{B2}$$

can be decomposed as follows

$$I_B = \lim_{\varepsilon \rightarrow 0} \int_{\Gamma_{\varepsilon}} t_{11}^{*T} u \, d\Gamma_{\varepsilon} = \lim_{\varepsilon \rightarrow 0} \int_{\Gamma_{\varepsilon}} \left\{ D \left[ \frac{\sqrt{\lambda_2} A_1}{z_2^2} - \frac{\sqrt{\lambda_1} A_2}{z_1^2} \right] (r_1 n_1 + r_2 n_2) \right\} d\Gamma_{\varepsilon}$$

where

$$I_{B1} = \lim_{\varepsilon \rightarrow 0} \int_{\Gamma_{\varepsilon}} t_{11}^{*T} u \, d\Gamma_{\varepsilon} = \lim_{\varepsilon \rightarrow 0} \int_{\Gamma_{\varepsilon}} \left\{ D \left[ \frac{\sqrt{\lambda_2} A_1}{z_2^2} \right] (r_1 n_1 + r_2 n_2) \right\} d\Gamma_{\varepsilon}$$

and

$$I_{B2} = \lim_{\varepsilon \rightarrow 0} \int_{\Gamma_\varepsilon} t_{11}^{*T} u \, d\Gamma_\varepsilon = - \lim_{\varepsilon \rightarrow 0} \int_{\Gamma_\varepsilon} \left\{ D \left[ \frac{\sqrt{\lambda_1} A_2}{z_1^2} \right] (r_1 n_1 + r_2 n_2) \right\} d\Gamma_\varepsilon$$

Using polar coordinates

$$\begin{cases} x = \zeta_1 + \varepsilon \cos \theta \\ y = \zeta_2 + \varepsilon \sin \theta \end{cases}$$

where

$$\begin{aligned} \varepsilon &= \sqrt{(x - \xi_1)^2 + (y - \xi_2)^2} \\ r_{,1} &= \frac{\partial r_1}{\partial x} = \frac{x - \xi_1}{\varepsilon} = \cos \theta \quad \longrightarrow \quad r_1 = \varepsilon \cos \theta \\ r_{,2} &= \frac{\partial r_2}{\partial y} = \frac{y - \xi_2}{\varepsilon} = \sin \theta \quad \longrightarrow \quad r_2 = \varepsilon \sin \theta \\ n &= [n_x, n_y] = [\cos \theta, \sin \theta] \\ d\Gamma &= \varepsilon d\theta \\ z_i &= \sqrt{\lambda_{1,2} (x - \xi_1)^2 + (y - \xi_2)^2} = \sqrt{\lambda_{1,2} (\varepsilon \cos \theta)^2 + (\varepsilon \sin \theta)^2} \end{aligned}$$

Then,  $\varepsilon \frac{x - \xi_1}{\varepsilon} = \varepsilon \cos \theta$  and taking in account (5),  $x - \xi_1 = r_1$  and  $y - \xi_2 = r_2$ . Therefore,

$$\begin{aligned} I_{B1} &= \\ &= D \sqrt{\lambda_2} A_1 \lim_{\varepsilon \rightarrow 0} \int_0^\pi \frac{\cos \theta^2 + \sin \theta^2}{\varepsilon^2 [1 + \cos^2 \theta (\lambda_2 - 1)]} u \, \varepsilon^2 d\theta = D \sqrt{\lambda_2} A_1 \frac{1}{\sqrt{\lambda_2}} \pi = \frac{A_1 u}{2(\lambda_1 - \lambda_2) S_{22}} \\ I_{B2} &= \\ &= -D \sqrt{\lambda_1} A_2 \lim_{\varepsilon \rightarrow 0} \int_0^\pi \frac{\cos \theta^2 + \sin \theta^2}{\varepsilon^2 [1 + \cos^2 \theta (\lambda_1 - 1)]} u \, \varepsilon^2 d\theta = -D \sqrt{\lambda_1} A_2 \frac{1}{\sqrt{\lambda_1}} \pi = -\frac{A_2 u}{2(\lambda_1 - \lambda_2) S_{22}} \end{aligned}$$

Finally,

$$I_B = I_{B1} + I_{B2} = \frac{A_1 - A_2}{2(\lambda_1 - \lambda_2) S_{22}} u = c_{11}$$

Therefore, the value of  $c_{11}$  for (14) is

$$c_{11} = \frac{A_1 - A_2}{2(\lambda_1 - \lambda_2) S_{22}} = c_{22}$$

Similarly, the term  $c_{22}$  results from integration of  $t_{22}$ , using the same procedure described above.

**Integration of  $t_{12}$  and  $t_{21}$** 

For integration of  $t_{12}$  and  $t_{21}$  we develop the following procedure

$$t_{12} = D \left\{ \left( \frac{\sqrt{\lambda_1} A_1}{z_1^2} - \frac{\sqrt{\lambda_2} A_2}{z_2^2} \right) r_1 n_2 - \left( \frac{\sqrt{\lambda_1} A_1}{\lambda_1 z_1^2} - \frac{\sqrt{\lambda_2} A_2}{\lambda_2 z_2^2} \right) r_2 n_1 \right\}$$

$$t_{12} = D \left\{ \sqrt{\lambda_1} A_1 \left( \frac{1}{z_1^2} r_1 n_2 - \frac{1}{\lambda_1} \frac{1}{z_1^2} r_2 n_1 \right) - \sqrt{\lambda_2} A_2 \left( \frac{1}{z_2^2} r_1 n_2 - \frac{1}{\lambda_2} \frac{1}{z_2^2} r_2 n_1 \right) \right\}$$

$$\int_{\Gamma} t_{12}^{*T} u \, d\Gamma = \lim_{\varepsilon \rightarrow 0} \left[ \underbrace{\int_{\Gamma - \Gamma_\varepsilon} t_{12}^{*T} u \, d(\Gamma - \Gamma_\varepsilon)}_{I_A} + \underbrace{\int_{\Gamma_\varepsilon} t_{12}^{*T} u \, d\Gamma_\varepsilon}_{I_B} \right]$$

where  $\varepsilon$  is distance between the source and field point. Let's consider

$$I_A = \lim_{\varepsilon \rightarrow 0} \int_{\Gamma - \Gamma_\varepsilon} t_{12}^{*T} u \, d(\Gamma - \Gamma_\varepsilon) = \int_{\Gamma} t_{12}^{*T} u \, d\Gamma$$

The term  $I_A$  is part of RHS of (14). This term has no singular contribution because it is away from the semi-circle in Fig. (19). Next,

$$I_B = \int_{\Gamma_\varepsilon} t_{12}^{*T} u \, d\Gamma_\varepsilon = I_{B1} + I_{B2}$$

can be decomposed as follows

$$I_B = \lim_{\varepsilon \rightarrow 0} \int_{\Gamma_\varepsilon} t_{12}^{*T} u \, d\Gamma_\varepsilon =$$

$$= \lim_{\varepsilon \rightarrow 0} \int_{\Gamma_\varepsilon} D \left\{ \sqrt{\lambda_1} A_1 \left( \frac{1}{z_1^2} r_1 n_2 - \frac{1}{\lambda_1} \frac{1}{z_1^2} r_2 n_1 \right) - \sqrt{\lambda_2} A_2 \left( \frac{1}{z_2^2} r_1 n_2 - \frac{1}{\lambda_2} \frac{1}{z_2^2} r_2 n_1 \right) \right\} d\Gamma_\varepsilon$$

where

$$I_{B1} = \lim_{\varepsilon \rightarrow 0} \int_{\Gamma_\varepsilon} t_{12}^{*T} u \, d\Gamma_\varepsilon = \lim_{\varepsilon \rightarrow 0} \int_{\Gamma_\varepsilon} D \left\{ \sqrt{\lambda_1} A_1 \left( \frac{1}{z_1^2} r_1 n_2 - \frac{1}{\lambda_1} \frac{1}{z_1^2} r_2 n_1 \right) \right\} d\Gamma_\varepsilon$$

and

$$I_{B2} = \lim_{\varepsilon \rightarrow 0} \int_{\Gamma_\varepsilon} t_{12}^{*T} u \, d\Gamma_\varepsilon = \lim_{\varepsilon \rightarrow 0} \int_{\Gamma_\varepsilon} -D \left\{ \sqrt{\lambda_2} A_2 \left( \frac{1}{z_2^2} r_1 n_2 - \frac{1}{\lambda_2} \frac{1}{z_2^2} r_2 n_1 \right) \right\} d\Gamma_\varepsilon$$

Using polar coordinates

$$I_{B1} =$$

$$= \lim_{\varepsilon \rightarrow 0} \int_0^\pi D \left\{ \sqrt{\lambda_1} A_1 \left( r_1 n_2 - \frac{1}{\lambda_1} r_2 n_1 \right) \right\} \frac{r}{z_1^2} u \, d\theta = -D \sqrt{\lambda_1} A_1 \lim_{\varepsilon \rightarrow 0} \int_0^\pi \frac{1}{z_1^2} \left\{ \left( \frac{1}{\lambda_1} r_2 n_1 - r_1 n_2 \right) \right\} \varepsilon u \, d\theta$$

$$I_{B2} =$$

$$= \lim_{\varepsilon \rightarrow 0} \int_0^\pi -D \left\{ \sqrt{\lambda_2} A_2 \left( r_1 n_2 - \frac{1}{\lambda_2} r_2 n_1 \right) \right\} \frac{r}{z_2^2} u \, d\theta = D \sqrt{\lambda_2} A_2 \lim_{\varepsilon \rightarrow 0} \int_0^\pi \frac{1}{z_2^2} \left\{ \left( \frac{1}{\lambda_2} r_2 n_1 - r_1 n_2 \right) \right\} \varepsilon u \, d\theta$$

$$\begin{aligned}
 I_{B1} &= -D\sqrt{\lambda_1}A_1 \lim_{\varepsilon \rightarrow 0} \int_0^\pi \frac{1}{z_1^2} \left\{ \left( \frac{1}{\lambda_1} \cos \theta \sin \theta - \cos \theta \sin \theta \right) \right\} \varepsilon^2 u d\theta = \\
 &= -D\sqrt{\lambda_1}A_1 \lim_{\varepsilon \rightarrow 0} \int_0^\pi \left\{ \left( \frac{1}{\lambda_1} - 1 \right) \frac{\cos \theta \sin \theta}{\varepsilon^2 [1 + \cos^2 \theta (\lambda_1 - 1)]} \right\} \varepsilon^2 u d\theta = 0 \\
 I_{B2} &= D\sqrt{\lambda_2}A_2 \lim_{\varepsilon \rightarrow 0} \int_0^\pi \frac{1}{z_2^2} \left\{ \left( \frac{1}{\lambda_2} \cos \theta \sin \theta - \cos \theta \sin \theta \right) \right\} \varepsilon^2 u d\theta = \\
 &= D\sqrt{\lambda_2}A_2 \lim_{\varepsilon \rightarrow 0} \int_0^\pi \left\{ \left( \frac{1}{\lambda_2} - 1 \right) \frac{\cos \theta \sin \theta}{\varepsilon^2 [1 + \cos^2 \theta (\lambda_2 - 1)]} \right\} \varepsilon^2 u d\theta = 0
 \end{aligned}$$

results in

$$c_{12} = c_{21} = 0$$

### Integration of kernels with singularity $O(\ln z_k)$

#### Integration of $u_{11}$ and $u_{22}$

For integration of  $u_{12}$  and  $u_{21}$  we use the following procedure

$$\int_\Gamma u_{11}^{*T} t d\Gamma = \lim_{\varepsilon \rightarrow 0} \left[ \underbrace{\int_{\Gamma-\Gamma_\varepsilon} u_{11}^{*T} t d(\Gamma - \Gamma_\varepsilon)}_{I_A} + \underbrace{\int_{\Gamma_\varepsilon} u_{11}^{*T} t d\Gamma_\varepsilon}_{I_B} \right]$$

where  $\varepsilon$  is distance between the source and field point. Expanding the two integrals on the RHS, we have

$$I_A = \lim_{\varepsilon \rightarrow 0} \int_{\Gamma-\Gamma_\varepsilon} u_{11}^{*T} t d(\Gamma - \Gamma_\varepsilon) = \int_\Gamma u_{11}^{*T} t d\Gamma$$

and

$$I_B = \lim_{\varepsilon \rightarrow 0} \int_{\Gamma_\varepsilon} u_{11}^{*T} t d\Gamma_\varepsilon = \lim_{\varepsilon \rightarrow 0} \int_{\Gamma_\varepsilon} D \left\{ \left[ \sqrt{\lambda_1} A_2^2 \ln z_1 - \sqrt{\lambda_2} A_1^2 \ln z_2 \right] \right\} t d\Gamma_\varepsilon$$

or

$$\begin{aligned}
 I_B &= \lim_{\varepsilon \rightarrow 0} \int_{\Gamma_\varepsilon} u_{11}^{*T} t d\Gamma_\varepsilon = \lim_{\varepsilon \rightarrow 0} \int_{\Gamma_\varepsilon} D \left[ \sqrt{\lambda_1} A_2^2 \ln z_1 \right] t d\Gamma_\varepsilon - \lim_{\varepsilon \rightarrow 0} \int_{\Gamma_\varepsilon} D \left[ \sqrt{\lambda_2} A_1^2 \ln z_2 \right] t d\Gamma_\varepsilon = \\
 &= D\sqrt{\lambda_1}A_2^2 \lim_{\varepsilon \rightarrow 0} \int_0^\pi \varepsilon^2 \ln \left[ \sqrt{1 + \cos^2 \theta (\lambda_1 - 1)} \right] t d\theta - D\sqrt{\lambda_2}A_1^2 \lim_{\varepsilon \rightarrow 0} \int_0^\pi \varepsilon^2 \ln \left[ \sqrt{1 + \cos^2 \theta (\lambda_2 - 1)} \right] t d\theta = 0
 \end{aligned}$$

### Integration of kernels with singularity $O(\arctan(r_2/\sqrt{\lambda_k}r_1))$

#### Integration of $u_{12} = u_{21}$

The integration procedure for  $u_{12}$  is as follows

$$\int_\Gamma u_{12}^{*T} t d\Gamma = \lim_{\varepsilon \rightarrow 0} \left[ \underbrace{\int_{\Gamma-\Gamma_\varepsilon} u_{12}^{*T} t d(\Gamma - \Gamma_\varepsilon)}_{I_A} + \underbrace{\int_{\Gamma_\varepsilon} u_{12}^{*T} t d\Gamma_\varepsilon}_{I_B} \right]$$

where  $\varepsilon$  is distance between the source and field point. Expanding the two integrals on the RHS, we have

$$I_A = \lim_{\varepsilon \rightarrow 0} \int_{\Gamma - \Gamma_\varepsilon} u_{12}^{*T} t d(\Gamma - \Gamma_\varepsilon) = \int_{\Gamma} u_{12}^{*T} t d\Gamma$$

and

$$I_B = \lim_{\varepsilon \rightarrow 0} \int_{\Gamma_\varepsilon} u_{12}^{*T} t d\Gamma_\varepsilon = \lim_{\varepsilon \rightarrow 0} \int_{\Gamma_\varepsilon} DA_1 A_2 \left[ \arctan \left( \frac{r_2}{\sqrt{\lambda_2} r_1} \right) - \arctan \left( \frac{r_2}{\sqrt{\lambda_1} r_1} \right) \right] t d\Gamma_\varepsilon$$

or

$$\begin{aligned} I_B &= \lim_{\varepsilon \rightarrow 0} \int_0^\pi u_{12}^{*T} t d\theta = \lim_{\varepsilon \rightarrow 0} \int_0^\pi DA_1 A_2 \left[ \arctan \left( \frac{\sin \theta}{\sqrt{\lambda_2} \cos \theta} \right) - \arctan \left( \frac{\sin \theta}{\sqrt{\lambda_1} \cos \theta} \right) \right] t \varepsilon d\theta = \\ &= \lim_{\varepsilon \rightarrow 0} \int_0^\pi DA_1 A_2 \left[ \left( \frac{\theta}{\sqrt{\lambda_2}} \right) - \left( \frac{\theta}{\sqrt{\lambda_1}} \right) \right] t \varepsilon d\theta = 0 \end{aligned}$$

## Acknowledgements

The authors wish to acknowledge the financial support from the RISPEISE cooperation project.

## References

- [1] Reddy JN. Mechanics of laminated Composite Plates and Shells, Theory and Analysis. CRC Press, second edition, 2004. Department of Mechanical Engineering at Texas A&M University, College Station, Texas, US.
- [2] Barbero EJ. Introduction to Composite Materials Design. Composite Materials: Analysis and Design. CRC Press, Boca Raton, FL, second edition, 2011. <http://barbero.cadec-online.com/icmd>.
- [3] Barbero E, Fernandez-Saez J, Navarro. Statistical analysis of the mechanical properties of composite materials. Compos Part B-Eng 2000; 31(5):375–381.
- [4] Giner E, Fernandez-Zuniga D, Fernandez-Saez J. On the jx1-integral and the out-of-plane constraint in a 3d elastic cracked plate loaded in tension. Int J Solids Struct 2010; 47(7-8):934–946.
- [5] Gonzalez-Albuixech VF, Giner E, Fernandez-Saez J. Influence of the t(33)-stress on the 3-d stress state around corner cracks in an elastic plate. Eng Fract Mech 2011; 78(2):412–427.
- [6] Loya JA, Rubio L, Fernandez-Saez J. Natural frequencies for bending vibrations of timoshenko cracked beams. J Sound Vib 2006; 290:3–5.
- [7] Rubio L, Fernandez-Saez J. A note on the use of approximate solutions for the bending vibrations of simply supported cracked beams. J Vib Acoust 2010; 132(2).
- [8] Barbero EJ. Finite Element Analysis of Composite Materials Using ANSYS. Composite Materials: Analysis and Design. CRC Press, Boca Raton, FL, 2014. <http://barbero.cadec-online.com/feacm-ansys>.

- [9] Barbero EJ, Zinno R. Analysis of laminated composite plates with three-dimensional layer-wise constant shear elements. *International Journal for Engineering Analysis and Design* 1994; 1:189–214.
- [10] Daghia F, de Miranda S, Ubertini F, Viola E. A hybrid stress approach for laminated composite plates within the first-order shear deformation theory. *Int J Solids Struct* 2008; 45(6):1766–1787.
- [11] de Miranda S, Patruno L, Ubertini F. Transverse stress profiles reconstruction for finite element analysis of laminated plates. *Compos Struct* 2012; 94(9):2706–2715.
- [12] de Miranda S, Ubertini F. A simple hybrid stress element for shear deformable plates. *Int J Numer Meth Eng* 2006; 65(6):808–833.
- [13] de Miranda S, Ubertini F. Stress analysis around holes or notches by special finite elements. *Int J Numer Meth Eng* 2006; 66(1):85–116.
- [14] Brebbia CA, Telles JCF, Wrobel LC. *Boundary element techniques*. Springer-Verlag, 1st ed edition, 1984. Berlin.
- [15] Brebbia CA, Dominguez J. *Boundary Elements: an introductory course*. McGraw-Hill Incorporated, 1st ed edition, 1989. London.
- [16] Hartmann F. *Introduction to Boundary Elements: Theory and Applications*. Springer-Verlag, 1st ed edition, 1989.
- [17] Aliabadi MH. *The Boundary Element Method, Volume 2, Application in Solids and Structures*. Wiley, second edition, 2002. Queen Mary, University of London, UK.
- [18] Pozrikidis C. *A Practical Guide to Boundary Element Methods with the Software Library BEMLIB*. CRC Press, first edition, 2002.
- [19] Banjai L. *Boundary Element Methods*. First edition, 2007. University of Zurich Institute of Mathematics, Herbstsemester, Zurich.
- [20] Banerjee PK, Butterfield R. *Boundary element methods in engineering science*. McGraw-Hill, first edition, 1981.
- [21] Katsikadelis JT. *Boundary Elements Theory and Applications*. Elsevier, first edition, 2002. Department of Civil Engineering, National Technical University of Athens, Athens, Greece.
- [22] Barone G, Pirrotta A, Santoro R. Cvbem solution for saint-venant orthotropic beams under coupled bending and torsion. *Acta Mech* 2015; 226(3):783–796.
- [23] Daros CH. The dynamic fundamental solution and bem formulation for laminated anisotropic kirchhoff plates. *Eng Anal Bound Elem* 2015; 54:19–27.
- [24] Hou PF, He S, Chen CP. 2d general solution and fundamental solution for orthotropic thermoelastic materials. *Eng Anal Bound Elem* 2011; 35(1):56–60.
- [25] Rajneesh K, Vijay C. Green's functions in orthotropic thermoelastic diffusion media. *Eng Anal Bound Elem* 2012; 36(8):1272–1277.

- [26] dos Reis A, Albuquerque EL, Palermo-Jr L. The boundary element method applied to orthotropic shear deformable plates. *Eng Anal Bound Elem* 2013; 37(4):738–746.
- [27] Useche J, Albuquerque EL, Sollero P. Harmonic analysis of shear deformable orthotropic cracked plates using the boundary element method. *Eng Anal Bound Elem* 2012; 36(11):1528–1535.
- [28] Cheng C, Han Z, Zhou H, Zhongrong N. Analysis of the temperature field in anisotropic coating-structures by the boundary element method. *Eng Anal Bound Elem* 2015; doi:10.1016/j.enganabound.2015.01.010.
- [29] di Pisa C, Aliabadi MH. Boundary element analysis of stiffened panels with repair patches. *Eng Anal Bound Elem* 2015; 56:162–175.
- [30] Foster TM, Mohamed MS, Trevelyan J, Coates G, Spence SH, Walker SK. Interactive three-dimensional boundary element stress analysis of components in aircraft structures. *Eng Anal Bound Elem* 2015; 56:190–200.
- [31] Magalhaes RR, Fontes CHO, Vieira de Melo SAB. Stress analysis of a front bumper fascia using the boundary element method. *Eng Anal Bound Elem* 2012; 36(8):1296–1300.
- [32] Balderrama R, Cisilino AP, Martinez M. Boundary element method analysis of three-dimensional thermoelastic fracture problems using the energy domain integral. *J Appl Mech* 2006; 73(6):959–969.
- [33] Cisilino AP. Topology optimization of 2d potential problems using boundary elements. *Comp Model Eng* 2006; 15(2):99–106.
- [34] Useche J, Albuquerque EL, Sollero P. Harmonic analysis of shear deformable orthotropic cracked plates using the boundary element method. *Eng Anal Bound Elem* 2012; 36(11):1528–1535.
- [35] Panzeca T, Parlavecchio E, Zito L. Lower bound limit analysis by bem: Convex optimization problem and incremental approach. *Eng Anal Bound Elem* 2013; 37(3):558–568.
- [36] Zito L, Parlavecchio E, Panzeca T. On the computational aspects of a symmetric multidomain boundary element method approach for elastoplastic analysis. *J Strain Anal Eng* 2011; 46(2):103–120.
- [37] Chen YC, Hwu C. Boundary element method for vibration analysis of two-dimensional anisotropic elastic solids containing holes, cracks or interfaces. *Eng Anal Bound Elem* 2014; 40:22–35.
- [38] Larrosa NO, Ortiz JE, Cisilino AP. Boundary element analysis of three-dimensional interface cracks in transversely isotropic bimetals using the Energy Domain Integral. *Key Eng Mat* 2011; 454:47–77.
- [39] Ortiz JE, Cisilino AP. Boundary element assessment of three-dimensional bimaterial interface cracks. *Fracture and Damage Of Composites* 2006; 8:249–288.
- [40] Green AE. A note on stress systems in anisotropic materials. *Philosophical Magazine* 1943; 34:416–418.

- [41] Rizzo RJ, Shippy DJ. A method for stress determination in plane anisotropic elastic bodies. *J Compos Mat* 1970; 4:36–61.
- [42] Huang L, Sun X, Liu Y, Cen Z. Parameter identification for two-dimensional orthotropic material bodies by the boundary element method. *Eng Anal Bound Elem* 2004; 28(2):109–121.
- [43] Szeidl G, Dudra J. Bem formulation for plane orthotropic bodies - a modification for exterior regions and its proof. *Periodica Polytechnica* 2007; 51(2):23–35.
- [44] Sun X, Huang L, Liu Y, Cen Z. Elasto-plastic analysis of two-dimensional orthotropic bodies with the boundary element method. *Tech Science Press* 2004; 1(1):91–105, 2004.
- [45] Sun X, Huang L, Liu Y, Cen Z. Boundary element analysis for elastic and elastoplastic problems of 2d orthotropic media with stress concentration. *Acta Mech Sinica* 2005; 22(5):472–484.
- [46] Sun X, Cen Z. Further improvement on fundamental solutions of plane problems for orthotropic materials. *Acta Mech Sinica* 2002; 15(2):171–181.
- [47] Michelitsch T, Levin VM. Green's function for the infinite two-dimensional orthotropic medium. *Int J Fracture* 2000; 107:33–38.
- [48] Aristodemo M, Turco E. A boundary element procedure for the analysis of two-dimensional elastic structures. *Boundary Integral Methods: theory and applications* 1990; 37:65–74.
- [49] Aristodemo M, Turco E. Boundary element discretization of plane elasticity and plate bending problems. *Int J Numer Meth Eng* 1994; 37:965–987.
- [50] Terravecchia S. Closed form coefficients in the symmetric boundary element approach. *Eng Anal Bound Elem* 2006; 30:479–488.
- [51] Gaspari D, Aristodemo M. Torsion and flexure analysis of orthotropic beams by a boundary element model. *Eng Anal Bound Elem* 2005; 29:850–858.
- [52] Zhou H, Niu Z, Cheng C, Guan Z. Analytical integral algorithm in the bem for orthotropic potential problems of thin bodies. *Eng Anal Bound Elem* 2007; 31:739–748.
- [53] Hartmann F. The somigliana identity on piecewise smooth surfaces. *J Elasticity* 1981, 11(4):403–423.
- [54] Kanwal RP. *Linear Integral Equations: theory and technique*. Birkhäuser, 2nd edition, 1996.
- [55] Aristodemo M. A high-continuity finite element model for two-dimensional elastic problems. *Comput-Struct* 1985; 21:987–993.
- [56] Danson DJ. A boundary element formulation of problems in linear isotropic elasticity with body forces. *Boundary element methods*. Springer, 1981.
- [57] Nowak AJ, Brebbia CA. The multiple-reciprocity method. a new approach for transforming bem domain integrals to the boundary. *Eng Anal Bound Elem* 1989; 6(3):164–167.
- [58] Neves AC, Brebbia CA. The multiple reciprocity boundary element method in elasticity: A new approach for transforming domain integrals to the boundary. *Int J Numer Meth Eng* 1991; 31(4):709–727.

- [59] Shippy DJ. Bem treatment of body forces in plane orthotropic elastostatics. *J Eng Mech* 1995; 121(10):1130–1135.
- [60] Zhang JJ , Tan CL , Afagh FF. A general exact transformation of body-force volume integral in bem for 2d anisotropic elasticity. *Comp Mech* 1996; 19(2):1–10.
- [61] Zhang J, Tan C, Afagh F. Treatment of body-force volume integrals in bem by exact transformation for 2-d anisotropic elasticity. *Int J Numer Meth Eng* 1997; 40(1):89–109.
- [62] Cheng AHD, Chen CS, Golberg MA. Bem for theomoeelasticity and elasticity with body force—a revisit. *Eng Anal Bound Elem* 2001; 25(4-5):377–387.
- [63] Guiggiani M. The evaluation of cauchy principal value integrals in the boundary element method, a-review. *Math Comput Model* 1991; 15:175–185.